OCA-B promotes pathogenic maturation of stem-like CD4+ T cells and autoimmune demyelination

Erik P. Hughes[1,3], Amber R. Syage[1,3], Elnaz Mirzaei Mehrabad[2,3,4], Thomas E. Lane[5], Benjamin T. Spike[2,3], Dean Tantin[1,3]

[1]Department of Pathology, University of Utah School of Medicine, Salt Lake City, UT, USA. [2]Department of Oncological Sciences, University of Utah School of Medicine, Salt Lake City, UT, USA. [3]Huntsman Cancer Institute, University of Utah School of Medicine, Salt Lake City, UT, USA. [4]School of Computing, University of Utah, Salt Lake City, UT, USA. [5]Department of Neurobiology and Behavior, School of Biological Sciences, University of California, Irvine, CA, USA.

Correspondence to Dean Tantin:
Department of Pathology, Division of Microbiology&Immunology
Huntsman Cancer Institute
University of Utah School of Medicine
Salt Lake City, UT 84112
dean.tantin@path.utah.edu
801-587-3035

Short title: OCA-B promotes CD4+ T cell mediated demyelinating disease

Keywords Adaptive immunity; OCA-B/Bob1/Pou2af1; autoimmunity; multiple sclerosis; experimental autoimmune encephalomyelopathy; CD4+ T cells; relapsing-remitting

Conflicts of interest statement: The authors have declared that no conflict of interest exists

Words in abstract: 193
Words main text: 11,637
Total main display items: 6

Abstract

Stem-like T cells selectively contribute to autoimmunity, but the activities that promote their pathogenicity are incompletely understood. Here, we identify the transcription coregulator OCA-B as a driver of the pathogenic maturation of stem-like $CD4^+$ T cell to promote autoimmune demyelination. Using two human multiple sclerosis (MS) datasets, we show that *POU2AF1*, the gene encoding OCA-B, is elevated in $CD4^+$ T cells from MS patients. We show that T cell-intrinsic OCA-B loss protects mice from experimental autoimmune encephalomyelitis (EAE) while preserving responses to viral CNS infection. In EAE models driven by antigen reencounter, OCA-B deletion nearly eliminates CNS infiltration, proinflammatory cytokine production and clinical disease. OCA-B-expressing $CD4^+$ T cells of mice primed with autoantigen express an encephalitogenic gene program and preferentially confer disease. In a relapsing-remitting EAE model, OCA-B loss protects mice specifically at relapse. During remission, OCA-B promotes the expression of *Tcf7*, *Slamf6*, and *Sell* in proliferating CNS T cell populations. At relapse timepoints, OCA-B loss results in both the accumulation of an immunomodulatory $CD4^+$ T cell population expressing *Ccr9* and *Bach2*, and loss of pro-inflammatory gene expression from Th17 cells. These results identify OCA-B as a driver of pathogenic $CD4^+$ T cells.

Introduction

2.8 million individuals worldwide suffer from multiple sclerosis (MS), with almost 1 million cases in the United States (1). Despite recent advances, the development of new therapies that block MS while sparing mechanisms that prevent infection and viral recrudescence remains a critical goal. Genome-wide association studies (GWAS) identify the *HLA* loci as the most important determinant of MS pathogenesis, emphasizing the impact of T cells (2, 3). The association with the major histocompatibility complex (MHC) class II locus in particular indicates that myelin-specific $CD4^+$ T cells are key regulators of disease.

The predominant preclinical model of MS is experimental autoimmune encephalomyelitis (EAE), in which laboratory animals are immunized with myelin proteins or peptides to activate antigen-specific $CD4^+$ T cells that infiltrate the central nervous system (CNS) and mediate disease. EAE within the C57BL/6 mouse background establishes chronic disease in which Th1 and Th17 effector $CD4^+$ T cell subsets are pathogenetic mediators (4, 5). After accessing the CNS, these cells secrete interferon-gamma (IFNγ), interleukin-17 (IL-17), granulocyte macrophage stimulating-factor (GM-CSF) and other inflammatory mediators and chemoattractants that recruit the cell types responsible for driving demyelination (6–8).

Myelin-reactive T cells from the blood of MS patients show stem/memory-like properties, with reduced need for co-stimulation (9–12). Consistent with these findings, autoreactive and bystander memory-phenotype $CD4^+$ T cells preferentially transfer demyelinating disease in mouse models (13–15). While these studies have identified vital $CD4^+$ T cell populations in EAE, further research on the mechanisms sustaining these populations and driving their pathogenic activity is required to develop more precise therapies.

Oct1, a POU domain transcription factor encoded by *Pou2f1*, has been linked to autoimmune disease. GWAS studies have identified Oct1 binding site polymorphisms that associate with a predisposition for autoimmune diseases, including MS (16–19). In $CD4^+$ T cells, Oct1 promotes the development of both $CD4^+$ memory (20) and EAE pathogenesis and demyelination (21). In contrast, Oct1 loss preserves immune responses to the neurotrophic viral infection (21). These observations highlight a promising pathway which when targeted may limit autoimmune CNS demyelination without the broad immune suppression elicited by many current therapeutics. However, Oct1 is widely expressed and regulates both embryonic development and somatic stem cell function (22–24), making it a poor therapeutic target.

The lymphoid-restricted transcription cofactor OCA-B regulates transcription by docking with Oct1, and in B cells an additional related factor, Oct2 (25). In B cells, OCA-B is essential for B cell maturation and germinal center formation (26–28). In contrast to Oct1, OCA-B whole-body

83 knockouts are viable and fertile (28). Polymorphisms in the *OCAB* (*POU2AF1*) locus are
84 associated with autoimmune diseases, including MS (29, 30). Although its expression is 50-100
85 fold lower in T cells compared to B cells (31), targeting either OCA-B by genetic deletion in T cells
86 or its downstream functions with a membrane-permeable peptide mimic suppresses type-1
87 diabetes (32). OCA-B interacts with target genes such as *Il2, Ifng, Il21, Csf2 (Gmcsf), Tnfrsf4*
88 *(Ox40), Icos* and *Ctla4*, but is dispensable for their expression following primary activation of T
89 cells. Instead, OCA-B regulates these targets under a narrow range of conditions, for example
90 following secondary stimulation in culture (20). Many of these targets are directly implicated in
91 MS pathogenesis (6–8, 33–39). OCA-B controls expression of *Tbx21* (*Tbet*), which encodes a
92 key regulator of Th1 effector responses, but also promotes Th17 differentiation and may interact
93 with RORγt, a master regulator of Th17 cells (20, 40, 41). In the context of MS, the only prior
94 OCA-B work used whole body knockouts and showed partial protection in chronic C57BL/6 EAE
95 models (41). Cumulatively, these findings indicate that OCA-B plays poorly defined but possibly
96 significant roles in MS pathogenesis.

97 Here, we show that OCA-B within the T cell compartment drives EAE by promoting
98 pathogenic maturation of stem-like $CD4^+$ T cells. In C57BL/6 mice, T cell OCA-B loss significantly
99 protects mice from chronic EAE while preserving responses to the neurotrophic coronavirus
100 JHMV. Using passive transfer assays in which reactive T cells are primed with antigen in donor
101 mice, polarized in culture, then reencounter antigen in naïve recipients, we show that OCA-B is
102 critical for the infiltration of pathogenic cells into the CNS and the manifestation of clinical disease.
103 Using an OCA-B reporter mouse, we find that OCA-B expressing $CD4^+$ T cells taken from MOG
104 peptide primed mice preferentially display pathogenic stem-like gene expression patterns and
105 preferentially transfer demyelinating disease, highlighting OCA-B as both a marker and promoter
106 of encephalitogenic autoimmune $CD4^+$ T cell activity. Intriguingly, T cell conditional OCA-B
107 knockout in EAE models on the autoimmune-prone non-obese diabetic (NOD) background, which
108 develop relapsing-remitting disease (42), specifically protects against relapse. Single-cell
109 transcriptomic analysis of $CD3\varepsilon^+$, CNS-infiltrating T cells at remission and relapse indicates that
110 OCA-B promotes disease relapse through control of stem-like T cell populations, driving them to
111 pathogenic Th17 differentiation. Cumulatively, these findings mark OCA-B as a critical mediator
112 of the pathogenic maturation of autoreactive T cells, and a promising potential therapeutic target.

113 Results

114 *Elevated expression of OCAB in CD4+ T cells from secondary-progressive human MS lesions.*
115 To determine if the gene encoding OCA-B is elevated in human MS samples, we mined high-
116 throughput single-nucleus RNA-seq data of glial and immune cells from a recent study using
117 single-nucleus RNA-seq to evaluate gene expression in brain tissue from 54 MS patients and 26
118 non-MS controls (43). The N=1 RRMS sample showed far higher *POU2AF1* expression
119 compared to CTR (Figure 1A). There were more primary-progressive (PPMS) samples, and
120 interestingly only one sample showed significant expression, perhaps reflecting imperfections in
121 diagnoses. Most dramatically, a subset of secondary-progressive (SPMS) samples showed
122 significantly elevated OCA-B expression (Figure 1A). We then reclustered $CD4^+$ cell nuclei from
123 this dataset. Uniform Manifold Approximation and Projection (UMAP) feature plots revealed that
124 the elevated *POU2AF1* found in T cell nuclei from SPMS patients was confined to one specific
125 $CD4^+$ cluster that also expresses the pathogenic marker *IL1R1* (Figure 1B). This cluster was also
126 marked by the expression of the T cell activation marker *CD44* and the transcription factors *LEF1*,
127 *ETS1*, *BCL6*, and *MAF* (Supplemental Figure 1A). To assess if elevated *POU2AF1* expression
128 was restricted to CNS infiltrating T cells, we analyzed recent bulk RNAseq dataset (44) comparing
129 peripheral blood memory T effector cells ("Teff", $CD4^+CD25^{low/neg}CD127^{hi}CD45RO^+$) from 20
130 RRMS patients and 20 healthy controls ("HC"). Similar to CNS T cells, *POU2AF1* expression in
131 peripheral $CD4^+$ T cells was found elevated in MS patients compared to non-MS controls
132 (Supplemental Figure 1B). These findings identify elevated *OCAB* mRNA expression in T cells
133 from MS patients across multiple datasets.

134 *OCA-B promotes chronic EAE in C57BL/6 mice.* To understand the impact of OCA-B in T
135 cell mediated autoimmunity, we utilized an *Ocab* conditional allele crossed to the CD4-Cre driver,
136 which efficiently deletes OCA-B in T cells (32). We induced EAE in C57BL/6 female $Ocab^{fl/fl}$;CD4-
137 Cre mice and littermate $Ocab^{fl/fl}$ controls through subcutaneous (s.c.) injection of myelin
138 oligodendrocyte glycoprotein $(MOG)_{35-55}$ peptide in Complete Freund's Adjuvant (CFA) followed
139 by intraperitoneal (i.p.) injections of *Bordetella pertussis* toxin. $Ocab^{fl/fl}$;CD4-Cre mice showed
140 reduced chronic EAE clinical scores and weight loss compared to $Ocab^{fl/fl}$ (Figure 1C-D). Spinal
141 cords were taken at peak disease (day 15) for immunofluorescence and histological analysis.
142 Myelin basic protein (MBP) immunofluorescence showed a significant decrease in demyelinated
143 white matter in spinal sections from $Ocab^{fl/fl}$;CD4-Cre mice compared to littermate $Ocab^{fl/fl}$ controls
144 while DAPI showed simultaneously decreased immune cell infiltration (Figure 1E-F). $Ocab^{fl/fl}$;CD4-
145 Cre mice also showed a significant decrease in demyelination as measured by luxol fast blue

146 (LFB) in combination with hematoxylin and eosin (H&E) staining (Supplemental Figure 2A-B).
147 Flow cytometric profiling at peak disease showed decreased $CD4^+$ T cell CNS infiltration using
148 *Ocab*$^{fl/fl}$;CD4-Cre mice, however no differences in other cell populations, anergic T cells
149 ($CD4^+FR4^+CD73^+$), or in the relative frequencies of the proinflammatory cytokines IFNy, IL-17,
150 GM-CSF, or CD44 were observed (Figure 1G-H and Supplemental Figure 2C-H). We studied
151 MOG-specific $CD4^+$ T cells using MHC class II (I-A^b) MOG_{38-49} tetramers. At peak disease,
152 *Ocab*$^{fl/fl}$;CD4-Cre mice showed a trending reduction in MOG tetramer-specific cell frequency
153 (p=0.055) and a significant reduction in numbers (p=0.003) compared to controls (Figure 1I-J).
154 These results indicate that the protection conferred by OCA-B loss in T cells is marked by modest
155 decreases in MOG-specific $CD4^+$ T cells within the CNS, resulting in fewer pathogenic T cells
156 driving demyelination.

157 *OCA-B is essential for EAE mediated by adoptive transfer of Th1- and Th17-polarized T*
158 *cells.* MS is driven by autoreactive $CD4^+$ Th1 and Th17 cells within the CNS that recruit $CD8^+$ T
159 cells, macrophages, microglia and neutrophils, which together mediate white-matter damage (45).
160 To investigate the impact of OCA-B on autoimmune Th1 and Th17 populations, we used adoptive
161 transfer EAE models with female *Ocab*$^{fl/fl}$;CD4-Cre and *Ocab*$^{fl/fl}$ littermate controls. Mice were
162 primed with MOG_{35-55} in CFA for 14 days. Following MOG priming, $CD4^+$ T cells were purified
163 from the lymph nodes of primed experimental or control donors (Supplemental Figure 3A). No
164 differences between genotypes in $CD4^+$ T cell viability, count, or effector cytokine (IFNγ and IL-
165 17) expression were observed (Supplemental Figure 3B-E).

166 To investigate if OCA-B expression impacts Th1 or Th17 mediated adoptive transfer EAE,
167 $CD4^+$ T cells purified from donors were polarized in vitro into Th1 and Th17 cells as previously
168 described (46, 47). 3×10^6 Th1- or Th17-polarized $CD4^+$ cells were transferred into naïve age-
169 matched wild-type male C57BL/6 recipients by i.p. injection. EAE onset in mice receiving either
170 Th1- or Th17-polarized control cells was rapid and severe (Figure 2A-B and Supplemental Figure
171 3F-G). In contrast to control cells, and in contrast to the mild protection observed with OCA-B
172 deficiency in standard C57BL/6 EAE, mice adoptively transferred with T cells lacking OCA-B were
173 almost completely protected from clinical disease regardless of their polarization state (Figure 2A-
174 and Supplemental Figure 3F-G). Interestingly, the ability to initially polarize $CD4^+$ T cells into Th1
175 and Th17 effectors in vitro was only minimally affected by OCA-B loss (Supplemental Figure 3H-
176 J), whereas cells taken from the CNS of engrafted recipient mice at day 15 not only showed
177 decreased CNS infiltration but also reduced IL-17 expression (Figure 2C-F). This effect appeared

178 to be specific to IL-17, as no significant difference in IFNγ was observed (Supplemental Figure
179 3K). These results indicate a central role for OCA-B in promoting robust neuroinflammatory T cell
180 responses upon antigen reencounter in adoptive transfer EAE models.

181 *OCA-B is dispensable for neurotropic viral clearance.* To investigate if T cell OCA-B
182 deletion impacts the ability to mount immune responses and control CNS viral infection, male
183 *Ocab*$^{fl/fl}$;CD4-Cre and *Ocab*$^{fl/fl}$ littermate controls were intracranially inoculated with 1500 plaque-
184 forming units (PFU) of the John H. Muller strain of murine hepatitis virus (JHMV), a β-coronavirus
185 adapted to infect glial cells (astrocytes, microglia and oligodendrocytes) in the mouse brain and
186 spinal cord. Inoculation with JHMV results in acute encephalomyelitis and chronic demyelination
187 similar to autoantigen-driven EAE. Disease severity was determined by evaluating clinical scores
188 over 21 days post-infection (dpi). *Ocab*$^{fl/fl}$;CD4-Cre animals showed negligible differences in
189 clinical scores compared to *Ocab*$^{fl/fl}$ littermates (Figure 3A). Spinal cords were taken on 12 and
190 21 dpi for immunofluorescence and histological analysis to investigate differences in
191 demyelination. MBP immunofluorescence at 12 dpi showed similar demyelination and immune
192 infiltration between Ocab$^{fl/fl}$ and Ocab$^{fl/fl}$;CD4-Cre spinal sections (Figure 3B-C). Similarly, LFB
193 histology of brain tissue at 21 dpi showed no significant differences in demyelination between
194 OCA-B deficient and control infected animals (Supplemental Figure 4A-B). Flow cytometric
195 analysis of brain tissue showed no significant differences in infiltrating CD4$^+$ T cell numbers or
196 IFNγ expression at 7, 12, or 21 dpi (Figure 3D-F, and Supplemental Figure 4C). Similarly, no
197 differences in either total CD8$^+$ T cell numbers, or the percentage or numbers of IFNγ-expressing
198 CD8$^+$ T cells was observed (Supplemental Figure 4D-F). Brain hemisphere homogenates were
199 collected on 7, 12 and 21 dpi to measure viral titers and clearance. *Ocab*$^{fl/fl}$;CD4-Cre and *Ocab*$^{fl/fl}$
200 littermate control animals showed similar titers at dpi 7 and 12, and virus was undetectable at day
201 21 regardless of genotype (Figure 3G). This result suggests that OCA-B is dispensable for
202 baseline immune responses to and clearance of neurotropic viruses.

203 *OCA-B expressing CD4$^+$ T cells display pathogenic stem-like properties and preferentially*
204 *transfer demyelinating disease.* We used a recently described OCA-B-mCherry reporter mouse
205 (31) to evaluate OCA-B expression within CNS infiltrating T cells. EAE was induced in female
206 C57BL/6 homozygous OCA-B-mCherry reporter mice with MOG_{35-55}, and CNS-infiltrating CD4$^+$ T
207 cells assessed by flow cytometry at peak clinical disease. mCherry-positive T cells showed
208 increased CD44 and CD62L co-expression, indicative of increased memory-like cells in the OCA-
209 B expressing population (Figure 4A). The association of OCA-B expression with a memory-like

210 profile was observed in the brain, spine and draining cervical lymph nodes (Figure 4B).
211 Interestingly, the frequency of $CD44^{+}CD62L^{-}CD4^{+}$ T cells was elevated within the OCA-B
212 expressing population specifically within the cervical lymph nodes (Supplemental Figure 5A).

213 Memory-like $CD4^{+}$ T cells have been implicated as major orchestrators of autoimmune
214 demyelination in mice and humans (9–12, 14, 15, 48). To see if this memory-like profile of OCA-
215 B expressing $CD4^{+}$ T cells is specific to CNS infiltrating cells, we performed flow cytometry using
216 draining lymph node and splenic T cells from MOG-primed OCA-B-mCherry reporter mice. Similar
217 to OCA-B^{+} CNS infiltrating cells, OCA-B expressing $CD4^{+}$ T cells taken from the cervical lymph
218 node and spleen showed increased CD44 and CD62L co-expression (Figure 4C-D).

219 We next evaluated OCA-B-mCherry positive and negative populations by RNA
220 sequencing (RNA-seq) of $CD4^{+}$ T cells isolated from the lymph nodes of 14-day MOG-primed
221 mice. $CD4^{+}$ T cells were sorted based on mCherry expression, as well as lack of CD8, lack of
222 CD19, expression of CD4 and viability (Supplemental Figure 5B). ~1500 genes were upregulated
223 and ~350 downregulated in OCA-B expressing compared to OCA-B negative cells (Supplemental
224 Table 1). Upregulated genes in OCA-B expressing cells included *Cxcr6*, *Slamf6*, *Il23r*, *Rorc*, *Ifng*,
225 *Bcl6*, and *Il17a* while downregulated genes included *Foxp3*, *Il7r* and *Ccr9* (Figure 4E-F).
226 Expression of *Tcf7* (which encodes TCF1) was high within both OCA-B positive and negative
227 populations (Supplemental Table 1). Gene ontology (GO) and pathway analysis of upregulated
228 genes show enrichment for terms associated with autoimmune diseases including lupus,
229 autoimmune thyroid disease, and type-1 diabetes (Figure 4G, and Supplemental Table 2). To
230 further assess how OCA-B may transcriptionally regulate these differentially regulated genes we
231 analyzed our previously published Oct1/OCA-B ChIPseq dataset (20). After realignment to the
232 *mm39* reference genome, Oct1 and OCA-B co-localized peaks were observed both near the
233 transcription start site as well as within gene body of *Tcf7*, *Bcl6*, and *Bach2* (Supplemental Figure
234 5C). These findings indicate that OCA-B likely directly regulates at least a subset of the
235 differentially expressed genes identified in gene knockout experiments.

236 To determine if OCA-B expression can be used to prospectively identify viable pathogenic
237 $CD4^{+}$ T cell populations, we used OCA-B-mCherry reporter mice as donors in passive transfer
238 EAE. 11-week-old male and female littermates homozygous for the OCA-B-mCherry reporter
239 were primed for 14 days with $MOG_{35\text{-}55}$ in CFA as previously described (47). 9×10^{5} mCherry
240 negative and positive cells were cultured in Th1 polarizing conditions and subsequently
241 transferred into age-matched male C57BL/6 recipients as previously described (14). Disease
242 progression was measured by clinical score and normalized weight. Recipients of OCA-B-

243 expressing, mCherry-positive cells showed increased clinical disease severity and weight loss
244 compared to mCherry-negative control recipients (Figure 4H and Supplemental Figure 5D). These
245 findings indicate that OCA-B marks $CD4^+$ T cells with pathogenic stem-like gene expression and
246 can be used to prospectively identify peripheral $CD4^+$ T cells with enhanced encephalitogenic
247 properties.

248 *OCA-B promotes neuroinflammation in relapsing-remitting EAE models via control of*
249 *stem/memory-like T cell populations.* In contrast to the chronic form of EAE that develops in
250 C57BL/6 mouse models, EAE on the NOD background exhibits a relapsing-remitting pattern that
251 more closely mimics human MS (42). We induced EAE in 15-18 week old female
252 NOD.*Ocab*$^{fl/fl}$;CD4-Cre and littermate control NOD.*Ocab*$^{fl/fl}$ mice (32) with MOG_{35-55}. Clinical
253 scores and weights were recorded for 47 days to observe initial disease onset, relapse and
254 relapse recovery. No significant differences in clinical scores were observed between groups at
255 disease onset (day 10-19), however following the primary remission, NOD.*Ocab*$^{fl/fl}$;CD4-Cre
256 animals were almost completely protected against disease relapse (Figure 5A). Individual NOD
257 mouse clinical scores are shown in Supplemental Figure 6. Normalized weights of animals also
258 reflected the protective effect of OCA-B loss in T cells at relapse (Figure 5B).

259 To understand differences in CNS-infiltrating T cells underlying relapse protection at a
260 population and transcriptional level, we performed single-cell RNA-seq (scRNA-seq) of $CD3\varepsilon^+$ T
261 cell isolates from CNS (brain + spinal cord) at remission (day 24) and peak relapse (day 33). Cells
262 from 3-6 NOD.*Ocab*$^{fl/fl}$;CD4-Cre and NOD.*Ocab*$^{fl/fl}$ littermate controls were collected and
263 combined for analysis. 7799 (remission) and 9224 (relapse) *Ocab* knockout, and 6009 (remission)
264 and 7525 (relapse) control cells passed filtering and were used for analysis, with an average per
265 cell read depth ranging from 90,000 to 190,000. For remission, UMAP clustering using both
266 genotypes revealed 16 clusters corresponding to a broad T cell repertoire consisting of natural-
267 killer T (NKT) cells (the largest cluster), $\gamma\delta$ T cells with a Th17-like gene signature (gd17), and
268 different $CD4^+$ and $CD8^+$ subsets (Figure 5C and Supplemental Figure 7A). Noteworthy clusters
269 based on mRNA expression included proliferating (*Ki67*, *Pcna*, *Mcm2*), Th1-like (*Tbx21*, *Ifng*, *Tnf*,
270 *Il12rb2*) and Treg (*Foxp3*, *Ctla4*, Supplemental Figure 7A-B and Supplemental Table 3). Feature
271 plots for *Foxp3* and *Mki67* are shown in Figure 5D. Additional feature plots for *Cxcr6*, *Il23r* and
272 *Bach2* are shown in Supplemental Figure 7C. *Bach2* was notably poorly expressed in all clusters,
273 in contrast to relapse timepoints (below). Notably, there was a large decrease in NKT cell numbers
274 in knockout mice (36% control vs. 14% experimental). Within this cluster, changes in gene

275 expression between control and conditional knockout groups were minimal. Most NKT cells from
276 both groups showed a limited inflammatory cytokine response, consistent with the lack of clinical
277 disease at remission. The decrease in the large NKT population in the experimental group
278 proportionally increases the percentage contribution of the other clusters, and therefore similar or
279 decreased percentages of these cells identifies reduced populations which correlate with
280 protection from relapse, e.g. proliferating T cells. Other clusters such as Tregs increased
281 disproportionately. Differential gene expression analysis of key clusters (Treg, Proliferating, and
282 Th1-like) revealed increased expression of *Slamf6* in Tregs lacking OCA-B, while OCA-B deficient
283 proliferating and Th1-like cells showed decreased expression of genes associated with
284 quiescence (*Btg1* and *Samhd1*), memory/stemness (*Slamf6*, *Tcf7*, and *Sell*) and pathogenicity
285 (*Tcf7* and *Tox* co-expression, Figure 5E). Spectral cytometry showed no significant difference in
286 the frequency of CNS infiltrating $CD4^+$ T cells between groups at remission (Figure 5F). However,
287 OCA-B deficient $CD4^+$ T cells did show a significant reduction in CXCR6 and IFNγ/GM-CSF co-
288 expression, indicative of reduced Th17 pathogenicity (Figure 5G-I). These results indicate that
289 loss of OCA-B in T cells selectively reduces proliferation and differentiation of pathogenic
290 stem/memory-like $CD4^+$ T cells during disease remission.

291 At relapse, multiple CNS-infiltrating stem-like and effector $CD4^+$ and $CD8^+$ control T cell
292 populations were present (Figure 6A and Supplemental Figure 8A-B, Supplemental Table 4). TCR
293 sequencing revealed an expansion of a subset of TCR clones in the OCA-B deficient CD8 clusters
294 while most other clusters were highly polyclonal (Figure 6B). Comparing the 10 most expanded
295 TCR clonotypes between knockouts and controls, there were several clonotypes that were shared
296 but differentially expanded (Supplemental Figure 8C and Supplemental Table 5). A "Ccr9 stem-
297 like" cluster expressing the gut homing chemokine receptor *Ccr9*, as well as *Ccr7*, *Bach2*, and
298 *Tcf7* notably appeared at relapse (Figure 6C and Supplemental Table 4). TCR clonotype analysis
299 indicated that this population was highly polyclonal (Figure 6B). Additionally, a "Stem-like CD4-2"
300 cluster expressing *Tcf7*, Ccr7, *Bach2, Cd44* and low-level *Cxcr6*, and a prominent "Th17-like"
301 cluster expressing *Tcf7, Cd44*, *Il1r1, Lgals3*, and higher levels of *Cxcr6* was identified (Figure 6C).
302 This latter cluster likely contains pathogenic effector cells.

303 In the absence of OCA-B, NKT cell populations were normalized compared to the
304 remission timepoint, and several clusters showed major changes in the percentage of cells
305 including most prominently within the Ccr9-stem-like cluster which was much more prevalent
306 (Figure 6D). Feature plots comparing OCA-B T cell deficient mice to littermate controls for *Ccr9*
307 and the transcription factors *Tcf7* and *Bach2* are shown in Figure 6D. The cells were also marked

308 by the expression of *Cd4*, *Tox, Ccr7, Ccr4* and limited expression of *Sell* (Supplemental Figure
309 9A).
310 RNA velocity analysis of spliced and unspliced transcripts (49) identified clusters of T cells,
311 most bearing static gene expression profiles consistent with terminal differentiation, but some with
312 differentiating or transitional gene expression (Figure 6E). Notably, OCA-B knockout cells showed
313 increased transcriptional stasis within the Ccr9-stem-like and proliferating clusters, and a
314 decreased transcriptional directionality of Th17 cells towards gd17 cells, the latter of which
315 express high levels of pathogenic markers including *Il1r1*, *Cxcr6*, and *Lgals3* (Supplemental
316 Figure 6A). Pseudotime analysis identified a transcriptional capacity in the control *Ccr9*
317 expressing population to differentiate into pathogenic Th17-like cells, whereas cells lacking OCA-
318 B were limited in this capacity, possibly resulting in the accumulation of these cells (Supplemental
319 Figure 9B). These changes culminated in the Th17-like effector knockout cells expressing
320 reduced pathogenicity-associated genes such as *Pdcd1*, *Tigit* and *Il1r1* (Figure 6F). Together
321 these results suggest OCA-B mediates the transition of non-pathogenic stem-like cells to
322 pathogenic Th17 cells which ultimately drive disease relapse.

323 Discussion

324 The development of therapies that inhibit autoimmunity while minimizing impacts on normal
325 immune function remains a critical unmet goal in the field. In this study, we show that expression
326 of mRNA encoding the transcriptional co-regulator OCA-B is elevated in CD4$^+$ T cells from SPMS
327 brain tissue and from effector memory-like peripheral blood CD4$^+$ T cells from RRMS patients.
328 We show that OCA-B promotes the pathogenic maturation of T cells and establishment of CNS
329 autoimmunity, in particular episodes of relapse. Loss of OCA-B attenuates these populations in
330 chronic EAE, in adoptive transfer EAE, and in NOD.EAE during remission. During relapse, OCA-
331 B T cell knockout mice are almost completely protected, and accumulate a population of CD4$^+$ T
332 cells expressing *Ccr9*, *Bach2*, and *Tcf7*. OCA-B expression also marks viable pathogenic
333 stem/memory-like CD4$^+$ T cells that preferentially transfer EAE. Furthermore, the effects of
334 modulating OCA-B are selective, as responses to infection with a neurotropic coronavirus that
335 generates similar clinical symptoms but lacks an autoantigen were largely unaffected.

336 OCA-B is a member of a small family of transcription co-regulators that also includes OCA-
337 T1, OCA-T2 and IκBζ (50, 51). It becomes induced upon CD4$^+$ T cell activation docks with Oct1
338 to directly regulate immunomodulatory genes such as *Il2*, *Ifng*, *Il17a*, Tbx21 (T-bet) and *Csf2*
339 (*Gmcsf*). Rather than functioning as a primary activator of these genes, it is required for their
340 robust expression upon antigen reencounter (20, 32). Notably, unlike transcription factors such
341 as NF-AT, AP-1 and NF-κB, Oct1 and OCA-B are dispensable for normal primary T cell responses
342 (20). These findings predict important roles for OCA-B in CD4$^+$ T cells specifically in situations of
343 antigen reencounter, which is a necessary feature of autoimmunity. Conditional T cell knockout
344 of Oct1 reduces EAE severity, with reduced proinflammatory cytokine expression and increased
345 anergy (21). Deletion of Oct1 in T cells was dispensable for neurotropic viral clearance (21),
346 however the ubiquitous expression of Oct1 in adult tissue limits its translational potential. In
347 contrast, OCA-B expression is largely confined to B and T cells, and whole-body knockout mice
348 are viable and fertile (52). OCA-B is highly expressed in B cells and required for germinal center
349 formation (52, 53). It is expressed in CD4$^+$ T cells at levels 50-100-fold less than in B cells (32,
350 54, 55). This suggests that with proper therapeutic dosing, OCA-B could be inhibited selectively
351 in T cells with minimal impact to the B cell compartment. Short-term administration of an OCA-B
352 peptide mimic that inhibits OCA-B's downstream effector functions reverses spontaneous type-1
353 diabetes in NOD mice (32). However, toxicity would limit the peptide mimic's efficacy, including in

354 EAE models. Further research is required for the development of safe and effective OCA-B
355 inhibitors.
356 OCA-B whole body knockout animals are partially protected from EAE (41), however, the
357 known activity of OCA-B in B cells made it unclear if the protection is T cell-derived. We show that
358 OCA-B promotes EAE pathogenesis through T cells. Opportunistic infections and reactivation of
359 latent CNS-tropic viruses are significant barriers for MS therapeutics that focus on global immune
360 suppression as a therapeutic mechanism. When OCA-B T cell conditional knockout mice are
361 challenged with the neurotropic coronavirus JHMV, there is little difference in their ability to mount
362 immune responses and control virus replication. These data are consistent with previous findings
363 that OCA-B loss in T cells preserves lymphocytic choriomeningitis virus (LCMV) acute viral
364 infection response, instead selectively impacting memory recall responses (20, 31). This finding
365 provides a potential therapeutic window in which targeting the low levels of OCA-B in T cells could
366 be used to blunt autoimmunity while sparing baseline immune responses.
367 Unlike the significant but modest protection observed in chronic C57BL/6 EAE, OCA-B
368 loss in adoptive transfer EAE almost completely protects recipient animals from disease. This
369 may indicate that adoptive transfer EAE models involve more autoantigen re-exposures, as
370 transferred T cells must re-encounter antigen in a naïve host before promoting disease. Protection
371 was observed regardless of whether donor cells were Th1- or Th17-polarized, indicating that
372 OCA-B functions through a mechanism that parallels rather than enforces the Th1/Th17
373 paradigm. We therefore sought other mechanisms that might explain why OCA-B T cell knockouts
374 are so strongly protected.
375 Autoimmune pathogenesis and maintenance has been increasingly associated with stem-
376 or progenitor-like T cell subpopulations (56, 57). Recent findings indicate an emerging role for
377 stem/memory-like T cells in promoting autoimmunity (48, 58–60). For example, myelin-specific
378 $CD4^+$ T cells in MS patients show signs of a previously activated, memory-like phenotype
379 compared to healthy controls (9, 10, 12). Furthermore, memory-like Th1 and Th17 cells are
380 increased in the peripheral blood of MS patients and display increased pathogenicity compared
381 to conventional Th17 Cells (61). Similarly, in EAE models, peripheral central memory-like
382 $CD4^+CD44^{hi}CD62L^{hi}$ T cells confer increased disease severity upon transfer (14). Both Oct1 and
383 OCA-B promote the functionality of long-lived $CD4^+$ memory T cells following antigenic
384 rechallenge (31, 62). An OCA-B-mCherry reporter mouse allele, which effectively labels memory
385 progenitor $CD4^+$ T cells during acute infection (31), also labels $CD4^+$ T cells that preferentially
386 confer EAE. OCA-B^{hi} cells taken from the CNS at peak EAE selectively express stem/memory

387 markers. Further profiling OCA-B^{hi} CD4^{+} T cells suggests that OCA-B promotes the transition of
388 non-pathogenic stem-like cells to a pathogenic state associated with markers such as *Cxcr6*,
389 *Slamf6*, *Ifng*, and *Il17a*. Elevated *Pou2af1* (*Ocab*) transcripts are also found in pathogenic Th17
390 cell populations (63). The connection between OCA-B expression and pathogenic memory/stem-
391 like T cells likely has not been appreciated before because OCA-B is expressed at levels too low
392 to be reproducibly captured with many current single-cell RNA-seq technologies.

393 Relapsing-remitting EAE models have been developed using the Swiss Jim Lambert (SJL)
394 and autoimmune prone non-obese diabetic (NOD) backgrounds (42, 64). In NOD mice, MOG_{35-55}
395 EAE has been described as relapsing-remitting with minimal initial disease that increases in
396 severity upon relapse (65, 66). Using this model with the conditional *Pou2af1* allele backcrossed
397 to the NOD background (32), we found that OCA-B T cell loss minimally affects initial clinical
398 presentation, but instead protects animals specifically at relapse. The finding that OCA-B loss in
399 conventional C57BL/6 EAE results in partial protection intermediate between the initial and
400 relapse phases of NOD.EAE suggests that chronic C57BL/6 EAE may not model either initial
401 presentation or relapse accurately, but instead represents a superposition of the two.
402 Nevertheless there are caveats associated with the NOD.EAE model, including poor
403 characterization relative to the C57BL/6 and SJL models, relatively weak clinical scores, lack of
404 temporal synchronic between replicate animals after the first relapse, and lack of underlying
405 progression (42, 67). Although we find that *POU2AF1* transcripts are elevated in T cells from
406 lesions of patients with secondary-progressive MS, more work is necessary for confirm selectivity
407 for OCA-B in promoting patient relapse and underlying progression.

408 Single-cell RNA expression profiling at remission identifies a significant loss of *Slamf6*,
409 *Tcf7* (encoding TCF1) and *Sell* from proliferative stem-like CD4^{+} T cells in the OCA-B deficient
410 condition. While the majority of research on TCF1-expressing stem-like T cells focuses on CD8^{+}
411 populations with the capacity for self-renewal and differentiation into effector cells, analogous
412 descriptions have been made for CD4^{+} populations (48, 68, 69). Indeed, autoimmune CD4^{+} T
413 cells expressing these memory/stem-like markers have been reported as an encephalitogenic
414 reservoir that play a key role in EAE pathogenicity (48). In the same study, bulk RNA sequencing
415 associated OCA-B expression within this stem-like reservoir (48).

416 Single-cell RNA-seq at relapse identified multiple emergent populations of effector T cells
417 compared to remission. Notably, there was also an accumulation of a unique population of CD4^{+}
418 cells in OCA-B T cell deficient mice. These cells are conspicuously marked by expression not
419 only of *Ccr4*, but also of *Ccr9*, which encodes a gut-homing chemokine receptor. CCR9^{+} memory-

420 like CD4$^+$ T cells have been linked to MS and EAE protection (70). The cells also express *Bach2*,
421 a transcription regulator which was recently associated with non-pathogenic immunomodulatory
422 Th17-polarized cells in the context of C57BL/6 EAE (71). *Bach2* expression was largely
423 concentrated in the "CCR9 stem-like" cluster, which is more numerous in the knockout condition.
424 Consistently, in bulk RNA-seq *Bach2* mRNA was upregulated in OCA-B$^-$ cells ($p<10^{-13}$), although
425 with a small (+1.74) fold change (Supplemental Table 1). Similarly, recent work associates
426 *Pou2af1* (*Ocab*) with pathogenic Th17/Th1 cells compared to the non-pathogenic *Bach2*
427 expressing cells (71). In B cells, OCA-B is known to regulate *Bach2* (72), however the interplay
428 between OCA-B and Bach2 and how this influences the pathogenic maturation of Th17 cells
429 merits additional research. Velocity and pseudotime analysis indicates that these cells are
430 normally transcriptionally inclined to progress towards an highly pathogenic Th17 population, but
431 that progression stalls in mice whose T cells lack OCA-B. Consistently, the Th17 effector
432 population in OCA-B T cell knockout mice lacks expression of key genes such as *Il1r1* and *Pdcd1*,
433 both of which are associated with pathogenicity in CNS-infiltrating Th17 cells[48,64]. The cumulative
434 alterations in these populations in OCA-B knockouts likely explains why these mice are strongly
435 protected against disease relapse. In conclusion, this study indicates a prominent role for OCA-B
436 in driving stem-like CD4$^+$ T cell populations towards a pathogenic state while playing a minimal
437 role in acute antiviral responses to a CNS infection.

438 Methods

439 *Sex as a biological variable.* The objective of this study was to determine the role of the
440 transcriptional regulator OCA-B in demyelinating disease. OCA-B T cell conditional knockout mice
441 and OCA-B reporter mice were utilized in multiple mouse demyelinating disease models to
442 evaluate the impact of T cell OCA-B expression on clinical disease manifestation and the
443 phenotypes of neuroinflammatory cells, in particular T cells. Both male and female animals were
444 used for experiments except for active EAE experiments where only female animals were used
445 as these are the better model spinal cord demyelination and inflammation.

446 *Analysis of publicly available human control and MS single nuclei RNAseq dataset.* Initial
447 evaluation of *POU2AF1* expression in T cells was conducted in the interactive web browser
448 created by the authors of the dataset available at https://malhotralab.shinyapps.io/MS_broad/
449 (43). Briefly, *POU2AF1* differential gene expression was filtered to show T cell gene expression
450 by diagnosis with a minimal threshold cutoff of 10 cells per sample. Cleaned aligned matrix files
451 were then downloaded from https://zenodo.org/records/8338963 and subsequently processed by
452 using the 10X Genomics CellRanger pipeline and further analyzed using the 10X Genomics
453 Loupe Browser 7 software. 19,906 $CD4^+$ cells were then subclustered and evaluated for
454 *POU2AF1* and *IL1R1* gene expression by diagnosis.

455 *Chronic C57BL/6 EAE.* 11-12 week-old female C57BL/6 littermate animals were used for
456 all experiments. For adoptive transfer experiments using the OCA-B-mCherry reporter allele (31),
457 11 week-old females were used for chronic EAE and 9 week-old males were used as MOG_{35-55}
458 primed adoptive transfer donors. EAE was induced on day 0 by two 100 μL s.c. injections into
459 both hind flanks of 0.5 μmol/mL MOG_{35-55} peptide (University of Utah Peptide Core) emulsified in
460 complete Freud's adjuvant (CFA), comprised of incomplete Freund's adjuvant (Cat#
461 77145;ThermoFisher) together with 4 mg/mL heat-killed *M. tuberculosis* (Cat#DF3114338, Fisher
462 Scientific). Animals were given two 400 ng i.p. injections of *B. pertussis* toxin (Cat#181, List
463 Biological Laboratories) on days 0 and 2.

464 *Clinical Scoring.* EAE clinical scores were determined using a 0-5 scale with 0.5 scoring
465 intervals: 0.5, tip of tail is limp or tail muscle strain observed; 1, complete limp tail; 1.5, complete
466 limp tail and at least one hind limb consistently falls through wire rack when animal is dropped; 2,
467 complete limp tail and one hind leg dragging without movement beyond hip; 2.5, complete limp
468 tail and dragging of both hind limbs without movement beyond hip; 3, complete hind limb paralysis;
469 3.5, complete hind limb paralysis with flat laying hind quarters and hump in upper torso; 4,

470 complete hind limb and partial forelimb paralysis, minimal movement around cage; 4.5, complete
471 hind limb and partial forelimb paralysis, no movement around cage; 5, seizure or death. Animals
472 scoring a ≥4 for more than 48 hr were euthanized and scored 5 for the remainder of the
473 experiment. JHMV clinical disease was evaluated using previously described 0-4 point scale (74).
474 *Immunofluorescence and Histology.* Spinal columns were isolated from C57BL/6 Ocab$^{fl/fl}$
475 and Ocab$^{fl/fl}$;CD4-Cre animals after EAE or JHMV induced demyelination and fixed overnight in in
476 4% paraformaldehyde at 4C. Spinal cords were subsequently isolated and cryoprotected in 30%
477 sucrose for 3-5 days. Thoracic and lumbar sections were embedded in optimum cutting
478 temperature (OCT) compound (ThermoFisher Scientific) and frozen and stored at -80C. 8 µm
479 spinal sections were cut by cryostat and stained with Luxol fast blue (Cat#212170250;
480 ThermoFisher) along with hematoxylin (Cat#8495; ENG Scientific) and eosin (Cat#E511-25;
481 Fisher Chemical). Demyelination was assessed by dividing the area of demyelinated white matter
482 by total white matter as previously described (75, 76). For immunofluorescence, spinal cord
483 sections were blocked in 5% normal goat serum (NGS; Cat#005-000-121, Jackson
484 ImmunoReseach) and 0.1% Tween-20 for 1 hr at room temperature. Sections were stained
485 overnight at 4°C with primary antibody rabbit anti-MBP (1:1000; Cat#PA1050, Boster), followed
486 by secondary antibody goat anti-rabbit conjugated with Alexa Fluor 488 (1:750; Cat#A11008,
487 Invitrogen) for 2 hr at room temperature. Primary and secondary antibodies were diluted in 1%
488 bovine serum albumin (BSA) and 0.1% Tween-20. Slides were cover-slipped using Fluoromount-
489 G with DAPI (Cat#00495952, Invitrogen). Sections were imaged with a Zeiss Axioscan 7
490 Microscope Slide Scanner using a 20× objective.
491 *Flow cytometry and spectral cytometry.* Spinal cords and brains were harvested at peak
492 disease or specified timepoint and mechanically dissociated by passing through a 100 µm cell
493 strainer. A 30/70% Percoll gradient (Cat#17544501, Cytiva) was used to enrich mononuclear
494 cells. Cells from collected spleens and lymph nodes (cervical, brachial, axillary and inguinal) were
495 passed through a 70 µm strainer and erythrocytes lysed by ammonium-chloride-potassium lysis
496 buffer (150 mM NH_4Cl, 10 mM $KHCO_3$, 0.1 mM Na_2EDTA). For intracellular staining, cells were
497 cultured in complete media (RPMI 1640, 10% FBS, 1% Pen/Strep, Glutamax) supplemented with
498 1 µL/mL brefeldin A (Cat#555029, Golgiplug, BD), 50 ng/mL phorbol myristate acetate (Cat#
499 P1585; Sigma-Aldrich) and 1 µg/mL ionomycin (Cat#I0634, Sigma-Aldrich) for 4 hr. Mouse I-A(b)
500 MOG_{38-49} tetramers (GWYRSPFSRVVH) (77, 78) and control I-A(b) Human CLIP tetramers
501 (PVSKMRMATPLLMQA) conjugated to APC or PE were synthesized by the National Institutes of

502 Health tetramer core facility. Cells were stained with control CLIP or MOG_{38-49} tetramers for 1 hr
503 at 37C prior to live/dead, surface, and intracellular staining. Cultured cells were fixed using
504 cytofix/cytoperm (Cat# 554714; BD) according to manufacturer's protocol and stained for
505 intracellular cytokines in perm/wash buffer. Antibodies used for flow cytometry include: CD45-
506 Percp(30F11, Cat#103129, Biolegend), CD11b-APC/Cy7(M1/70, Cat#101225, Biolegend),
507 CD19-BUV661(ID3, Cat#612971, BD), CD19-FITC(103/CD19, Cat#152404, Biolegend), NK1.1-
508 PE-Cy5(PK136, Cat#108715, Biolegend), CD3e-BV605(17A2, Cat#100237, Biolegend), CD3e-
509 FITC(145-2C11, Cat#100305, Biolegend), TCRb-BV570(H57-597, Cat#109231, Biolegend),
510 CD4-BV711(RM4-5, Cat#100557, Biolegend), CD4-BUV395(GK1.5, Cat#565974, BD), CD8a-
511 APC(53-6.7, Cat#100712, Biolegend), CD8a-BUV737(53-6.7, Cat#612759, BD), I-A/I-E-
512 BUV805(M5/144.15.2, Cat#748844, BD), CD62L-PE-Cy7(MEL-14, Cat#25-0621-82,
513 eBioscience), CD44-Percp-Cy5.5(IM7, Cat#45-0441-80, eBioscience), Ly-108-BUV563(13G3,
514 Cat#7741436, BD), FR4-BUV496(12A5, Cat#750415, BD), CD73-V450(Ty/23, Cat#561544, BD),
515 IL-23R-BV421(12B2B64, Cat#150907, Biolegend), CXCR6-BV711(SA051D1, Cat#151111,
516 Biolegend), PD-1-APC/Fire810(29F.1A12, Cat#135251, Biolegend), IFNγ-PE-Cy7(XMG1.2,
517 Cat#25-7311-82, eBioscience), IFNγ-APC(XMG1.2, Cat#17-7311-81, eBioscience), IL-17a-
518 BV605(TC11-18H10.1, Cat#506927, Biolegend), IL-17a-BV650(TC11-18H10.1, Cat#506929,
519 Biolegend), TNFa-FITC(MP6-XT22, Cat#506304, Biolegend), and GMCSF-PE/Dazzle594(MP1-
520 22E9, Cat#505421, BioLegend). Flow cytometry samples were profiled using a BD Fortessa (BD
521 Biosciences, Figure 2, 3, 4) or an Aurora spectral flow cytometer (Cytek, Fig 1 and 5). FlowJo
522 software (BD Biosciences) was used for data analysis.

523 *Pre-polarization profiling and mixed adoptive transfer.* 10 week-old C57BL/6 *Ocab*$^{fl/fl}$ and
524 *Ocab*$^{fl/fl}$*;CD4-Cre* littermates were immunized with MOG_{35-55} in CFA as described above. After 14
525 days, spleen and lymph node (cervical, axillary, brachial and inguinal) cells were isolated and
526 cultured in complete media (RPMI 1640, 10% FBS, 1% Pen/Strep, Glutamax) supplemented with
527 1 µL/mL brefeldin A (Cat#555029; Golgiplug, BD), 50 ng/mL phorbol myristate acetate
528 (Cat#P1585; Sigma-Aldrich) and 1 µg/mL ionomycin (Cat#I0634, Sigma-Aldrich) for 4 hr. Cells
529 were stained for surface markers, fixed using the Foxp3/Transcription Factor Staining Buffer Kit
530 (Cat#00-5523-00, ThermoFisher), and stained for intracellular markers (IFNγ and IL-17).

531 *Th1 and Th17 polarization and adoptive transfer C57BL/6 EAE.* 10-12 week-old female
532 C57BL/6 littermate animals were used for all experiments. Donor animals were immunized with
533 MOG_{35-55} in CFA as above. 10-14 days post-immunization, spleen and lymph node (cervical,

534 axillary, brachial and inguinal) cells were collected and placed into mixed culture with MOG
535 peptide and cytokines at 5.0×10^6 cells/mL. For Th1 conditions, complete media was
536 supplemented with 50 μg/mL MOG_{35-55}, 6 ng/mL rmIL-6 (Cat#216-16, Peprotech) and 2 ng/mL
537 rmIFNγ (Cat#315-05, Peprotech). For Th17 conditions, complete media was supplemented with
538 50 μg/mL MOG_{35-55}, 8 ng/mL rmIL-23 (Cat#1887-ML-010, R&D Systems), 10 ng/mL rmIL-1α
539 (Cat#211-11A, Peprotech), and 10 μg/mL anti-IFNγ (Cat#BE0055, BioXcell XMG1.2). After 4 days
540 of respective culture, $CD4^+$ T cells were purified using negative magnetic selection and
541 resuspended in PBS at 1.5×10^6 cells/mL. 100 μL cell suspension was injected i.p. into age-
542 matched male C57BL/6 recipients (~13 week-old at time of disease induction). Clinical disease
543 was scored for 15 days.

544 *JHMV. Ocab$^{fl/fl}$* and *Ocab$^{fl/fl}$*;CD4-Cre C57BL/6 mice were anesthetized using isoflurane.
545 Mice were intracranially (i.c) injected with 1500 plaque-forming units (PFU) of JHMV (strain V34)
546 suspended in 30 μL Hank's balanced salt solution (ThermoFisher). Clinical disease was assessed
547 for 21 days using a previously described scale (74). Mice were sacrificed at days 7, 12, and 21
548 post-infection to assess viral titers within brain homogenates using a plaque assay previously
549 described (79). Spinal cords were taken on day 12 and 21 post-infection to assess demyelination
550 by DAPI/MBP and luxol fast blue and hematoxylin/eosin histology respectively.

551 *OCA-B-mCherry adoptive transfer EAE.* OCA-B-mCherry reporter allele animals (31) were
552 primed for 14 days with MOG_{35-55} in CFA as described above. After priming, spleen and lymph
553 nodes were collected and $CD4^+$ T cells were purified by magnetic negative selection (Miltenyi Bio
554 kit and LS columns). Non-$CD4^+$ T cells were removed from the LS column and placed on ice for
555 subsequent in vitro culture. Purified $CD4^+$ T cells were separated by OCA-B-mCherry expression
556 (PE-Texas Red) using flow automated cell sorting (FACS) on a BD Aria cell sorter. OCA-B-
557 mCherry positive and negative $CD4^+$ T cells were placed into mixed culture in complete medium
558 with the previously purified non-$CD4^+$ T cells at a 1:10 ratio ($CD4^+$ to non-$CD4^+$) at 1.0×10^6
559 cells/mL. The culture was supplemented with 20 μg/mL MOG_{35-55} and 0.5 ng/mL IL-12p70
560 (Cat#210-12, Peprotech). After two days of culture, $CD4^+$ T cells were again purified through
561 negative magnetic selection. Purified $CD4^+$ T cells from OCA-B-mCherry positive and negative
562 cultures were resuspended in PBS at 8.8×10^6 cells/mL. 100 μL cell suspension was injected i.p.
563 into age-matched male C57BL/6 recipients. Clinical disease was assessed for 24 days.

564 *Bulk RNA-seq.* OCA-B-mCherry reporter mice (n=9) were primed for 14 days with MOG_{35-}
565 $_{55}$ in CFA as described above. After priming, lymph nodes (cervical, axillary, brachial and inguinal)

566 were isolated and mCherry positive and negative $CD4^+$ T cells were collected by FACS. Total
567 RNA, three groups (pooled 3 mice each), was isolated using the Quick RNA micro kit (Cat#
568 R1050; Zymo Research) with DNase treatment (Cat#79254, Qiagen). RNA concentration was
569 measured with a Qubit RNA HS Assay Kit (Cat#Q32855, Fisher Scientific). RNA quality was
570 evaluated with an RNA ScreenTape Assay (Cat#5067-5579, 5067-5580, Agilent Technologies).
571 Total RNA samples (5-500 ng) were hybridized with NEBNext rRNA Depletion Kit v2 (Cat#E7400,
572 New England Biolabs) to diminish rRNA from the samples. Stranded RNA sequencing libraries
573 were prepared as described using the NEBNext Ultra II Directional RNA Library Prep Kit for
574 Illumina (Cat#E7760L; New England Biolabs). Purified libraries were qualified on an 4150
575 TapeStation (Agilent Technologies) using a D1000 ScreenTape assay (Cat#5567-5582, 5067-
576 5583, Agilent Technologies). The molarity of adapter-modified molecules was defined by
577 quantitative PCR using the Kapa Biosystems Kapa Library Quant Kit (Cat#KK4824, Roche).
578 Individual libraries were normalized to 5 nM. NovaSeq 150×150 bp sequencing libraries were
579 chemically denatured and applied to an Illumina NovaSeq flow cell using the XP workflow
580 (20043131). Following transfer to an Illumina NovaSeq 6000 instrument, 150×150 cycle paired-
581 end sequencing was performed using a S4 reagent Kit v1.5 (Cat#20028312, Illumina). 8-11 million
582 reads were generated per sample and were aligned to the *GRCm38* mouse reference genome.
583 Differential gene expression and pathway analysis were conducted using the DESeq2 and Enrichr
584 R packages.

585 *NOD-EAE.* 15-18 week-old female littermate *Ocab*$^{fl/fl}$ and *Ocab*$^{fl/fl}$;CD4-Cre animals
586 backcrossed to a NOD strain background (32) were used for all experiments. Diabetic mice (blood
587 glucose >150 mg/dL) were excluded from the analysis. EAE was induced by two 100 μL s.c.
588 injections into both hind flanks of 0.5 μmol/mL MOG_{35-55} peptide emulsified in incomplete Freuds
589 adjuvant (Cat#77145, ThermoFisher) supplemented with 4 mg/mL heat-killed *M. tuberculosis*
590 (Cat#DF3114338, Fisher Scientific) to form CFA. Animals were given two 400 ng i.p. injections of
591 *Bordetella pertussis* toxin (Cat#181, List Biological Laboratories) on days 0 and 2. Clinical disease
592 was assessed over 47 days using the same 5-point scale described above. Remission timepoints
593 were determined to be between days 22-26 while first relapse was determined to be between
594 days 26-39.

595 *Single-cell RNA-seq.* NOD.*Ocab*$^{fl/fl}$ and NOD.*Ocab*$^{fl/fl}$;CD4-Cre animals were induced with
596 EAE and monitored for disease progression. Brains and spinal cords were isolated on day 24
597 (remission) and day 33 (relapse), and processed for FACS sorting. Viable cells were sorted by

598 CD3ε using a FACSAria (BD Bioscience). Cells from each condition were isolated from 3-4 mice
599 and combined. Cells were processed using the 5' 10X Genomics Chromium platform according
600 to the manufacturer's instructions. Paired-end high-throughput sequencing (125 cycles) was
601 performed using a NovaSeq instrument (Illumina). Sequencing reads were processed by using
602 the 10X Genomics CellRanger pipeline and further analyzed using the Seurat R package.
603 Analysis of cells used a standard filtering protocol removing cells with unique feature counts of
604 >5,000 or <100, as well as cells with >10% mitochondrial counts (indicative of dead cells). No
605 more than 10% of total cells were removed by this process. Cells were subjected to unsupervised
606 hierarchical clustering followed by uniform manifold approximation and projection (UMAP) to
607 visualize clusters with similar gene expression and their relative positions. RNA velocity analysis
608 was performed using velocyto.R version 0.6 to model cell state transitions using the guidelines
609 provided in Manno et al. (49) and the associated repository at https://github.com/velocyto-
610 team/velocyto.R. High dimensional velocity vectors were graphed on the predefined Seurat
611 UMAP projection using localized average grid projections. Pseudotime analysis was conducted
612 using Seurat and Monocle3 packages. Integrated data was divided into subset based on genotype
613 and Monocle3 was used to calculate trajectory, order cells and plot pseudotime for each condition.
614 *Statistics.* Multiple two-tailed student's t-tests were used to determine statistical
615 differences in EAE clinical scores and all error bars denote ±SEM unless otherwise noted. Two-
616 way ANOVA was used to determine differences in weight loss throughout disease progression.
617 GraphPad Prism software was used for all statistics and graphing. Two-tailed student's t-tests
618 were used to determine statistical differences in cell populations observed by flow cytometry and
619 all error bars represent ±SD unless otherwise noted. For all figures, ns = $p>0.05$, * = $p\leq0.05$, ** =
620 $p\leq0.01$, *** = $p\leq0.001$, **** = $p\leq0.0001$.
621 *Study approval.* All animal experiments were performed in strict accordance with the NIH
622 guide for the Care and Use of Laboratory animals and institutional guidelines for animal care at
623 the University of Utah under approved protocol #00001553.
624 *Data availability.* All RNA sequencing, single-cell sequencing, and single-cell T cell V(D)J
625 sequencing data associated with the findings of this study have been deposited to NCBI's GEO
626 database under accession code GSE243727. Data values for all graphs and values behind any
627 reported means are located in the Supporting Data Values file.
628
629

630 Author contributions

631 E.P.H. and D.T. conceived the study. E.P.H. and A.S. performed experiments. E.P.H,
632 A.S., E.M.M. and B.T.S. analyzed data. T.E.L., B.T.S. and D.T. provided critical resources and
633 supervision for the study. E.P.H. and D.T. wrote, reviewed and revised the manuscript.

634

635 Acknowledgements

636 We thank R.M. O'Connell and M. Bettini for critical reading of the manuscript. We thank J.
637 Marvin and University of Utah Health Sciences Center Flow Cytometry core, and B. Dalley, O.
638 Allen and the High-Throughput Genomics core. Peptides were synthesized by the DNA/Peptide
639 facility. We thank T. Lane for assistance with JHMV constructs, protocols and reagents. This work
640 was supported by grants from the National Institutes of Health/ National Institute of Allergy and
641 Infectious Diseases (R01AI162929 and R01AI100873) and the Praespero Foundation (Canada)
642 to DT, and training grants from the National Institute of Neurological Disorders and Stroke
643 (T32NS115664) to EPH and National Institute of Allergy and Infectious Diseases (T32AI055434)
644 to ARS.

645

646 **References**

647 1. Walton C, et al. Rising prevalence of multiple sclerosis worldwide: Insights from the Atlas of
648 MS, third edition. *Mult Scler J*. 2020;26(14):1816–1821.
649 2. Wtccc CC, et al. Genetic risk and a primary role for cell-mediated immune mechanisms in
650 multiple sclerosis. *Nature*. 2011;476(7359):214–219.
651 3. IMSGC. A high-density screen for linkage in multiple sclerosis. *Am J Hum Genet*.
652 2005;77(3):454–467.
653 4. Adorini L, Guery J-C, Trembleau S. Manipulation of the Th1/Th2 Cell Balance: An Approach
654 to Treat Human Autoimmune Diseases? *Autoimmunity*. 1996;23(1):53–68.
655 5. Langrish CL, et al. IL-23 drives a pathogenic T cell population that induces autoimmune
656 inflammation. *J Exp Med*. 2005;201(2):233–240.
657 6. Brucklacher-Waldert V, et al. Phenotypical and functional characterization of T helper 17 cells
658 in multiple sclerosis. *Brain*. 2009;132(12):3329–3341.
659 7. Montes M, et al. Oligoclonal myelin-reactive T-cell infiltrates derived from multiple sclerosis
660 lesions are enriched in Th17 cells. *Clin Immunol*. 2009;130(2):133–144.
661 8. Hartmann FJ, et al. Multiple sclerosis-associated IL2RA polymorphism controls GM-CSF
662 production in human TH cells. *Nat Commun*. 2014;5(1):5056.
663 9. Scholz C, et al. Expansion of Autoreactive T Cells in Multiple Sclerosis Is Independent of
664 Exogenous B7 Costimulation. *J Immunol*. 1998;160(3):1532–1538.
665 10. Burns JB, Bartholomew BD, Lobo ST. Isolation of CD45RO+, Memory T Cells Recognizing
666 Proteolipid Protein from Neurologically Normal Subjects. *Cell Immunol*. 2001;212(1):44–50.
667 11. Pelfrey CM, et al. Quantification of Self-Recognition in Multiple Sclerosis by Single-Cell
668 Analysis of Cytokine Production. *J Immunol*. 2000;165(3):1641–1651.
669 12. Lovett-Racke AE, et al. Decreased dependence of myelin basic protein-reactive T cells on
670 CD28-mediated costimulation in multiple sclerosis patients. A marker of activated/memory T
671 cells. *J Clin Invest*. 1998;101(4):725–730.
672 13. Lee H-G, et al. Pathogenic function of bystander-activated memory-like CD4+ T cells in
673 autoimmune encephalomyelitis. *Nat Commun*. 2019;10(1):709.
674 14. Williams JL, et al. Memory cells specific for myelin oligodendrocyte glycoprotein (MOG)
675 govern the transfer of experimental autoimmune encephalomyelitis. *J Neuroimmunol*.
676 2011;234(1–2):84–92.
677 15. Elyaman W, et al. Distinct Functions of Autoreactive Memory and Effector CD4+ T Cells in
678 Experimental Autoimmune Encephalomyelitis. *Am J Pathol*. 2008;173(2):411–422.

679 16. Maurano MT, et al. Systematic Localization of Common Disease-Associated Variation in
680 Regulatory DNA. *Science (80-)*. 2012;337(6099):1190–1195.
681 17. Graham DSC, et al. Evidence for unique association signals in SLE at the CD28–CTLA4–
682 ICOS locus in a family-based study. *Hum Mol Genet*. 2006;15(21):3195–3205.
683 18. van Heel DA. Inflammatory bowel disease is associated with a TNF polymorphism that
684 affects an interaction between the OCT1 and NF-kappaB transcription factors. *Hum Mol Genet*.
685 2002;11(11):1281–1289.
686 19. Farh KK, et al. Genetic and epigenetic fine mapping of causal autoimmune disease variants.
687 *Nature*. 2015;518(7539):337–343.
688 20. Shakya A, et al. Oct1 and OCA-B are selectively required for CD4 memory T cell function. *J*
689 *Exp Med*. 2015;212(12):2115–2131.
690 21. Kim H, et al. T cell-selective deletion of Oct1 protects animals from autoimmune
691 neuroinflammation while maintaining neurotropic pathogen response. *J Neuroinflammation*.
692 2019;16(1):133.
693 22. Vázquez-Arreguín K, et al. Oct1/Pou2f1 is selectively required for colon regeneration and
694 regulates colon malignancy. *PLOS Genet*. 2019;15(5):e1007687.
695 23. Perovanovic J, et al. Oct1 cooperates with the Smad family of transcription factors to
696 promote mesodermal lineage specification. *Sci Signal*. 2023;16(781).
697 https://doi.org/10.1126/scisignal.add5750.
698 24. Sebastiano V, et al. Oct1 regulates trophoblast development during early mouse
699 embryogenesis. *Development*. 2010;137(21):3551–3560.
700 25. Hwang SS, et al. Role of OCT-1 and partner proteins in T cell differentiation. *Biochim*
701 *Biophys Acta - Gene Regul Mech*. 2016;1859(6):825–831.
702 26. Teitell MA. OCA-B regulation of B-cell development and function. *Trends Immunol*.
703 2003;24(10):546–53.
704 27. Shi W, et al. Transcriptional profiling of mouse B cell terminal differentiation defines a
705 signature for antibody-secreting plasma cells. *Nat Immunol*. 2015;16(6):663–73.
706 28. Kim U, et al. The B-cell-specific transcription coactivator OCA-B/OBF-1/Bob-1 is essential
707 for normal production of immunoglobulin isotypes. *Nature*. 1996;383(6600):542–547.
708 29. The GAMES Collaborative Group. Linkage disequilibrium screening for multiple sclerosis
709 implicates JAG1 and POU2AF1 as susceptibility genes in Europeans. *J Neuroimmunol*.
710 2006;179(1–2):108–116.
711 30. Nakamura M, et al. Genome-wide Association Study Identifies TNFSF15 and POU2AF1 as

712 Susceptibility Loci for Primary Biliary Cirrhosis in the Japanese Population. *Am J Hum Genet*.
713 2012;91(4):721–728.
714 31. Sun W, et al. OCA-B/Pou2af1 is sufficient to promote CD4+ T cell memory and
715 prospectively identifies memory precursors. *Proc Natl Acad Sci U S A*.
716 2024;121(9):e2309153121.
717 32. Kim H, et al. Targeting transcriptional coregulator OCA-B/Pou2af1 blocks activated
718 autoreactive T cells in the pancreas and type 1 diabetes. *J Exp Med*. 2021;218(3):133.
719 33. Tzartos JS, et al. IL-21 and IL-21 Receptor Expression in Lymphocytes and Neurons in
720 Multiple Sclerosis Brain. *Am J Pathol*. 2011;178(2):794–802.
721 34. Ndhlovu LC, et al. Critical Involvement of OX40 Ligand Signals in the T Cell Priming Events
722 During Experimental Autoimmune Encephalomyelitis. *J Immunol*. 2001;167(5):2991–2999.
723 35. Hurwitz AA, et al. Cytotoxic T lymphocyte antigen-4 (CTLA-4) limits the expansion of
724 encephalitogenic T cells in experimental autoimmune encephalomyelitis (EAE)-resistant BALB/c
725 mice. *Proc Natl Acad Sci*. 2002;99(5):3013–3017.
726 36. Arellano G, et al. Stage-Specific Role of Interferon-Gamma in Experimental Autoimmune
727 Encephalomyelitis and Multiple Sclerosis. *Front Immunol*. 2015;6(SEP).
728 https://doi.org/10.3389/fimmu.2015.00492.
729 37. Rottman JB, et al. The costimulatory molecule ICOS plays an important role in the
730 immunopathogenesis of EAE. *Nat Immunol*. 2001;2(7):605–611.
731 38. Rouse M, Nagarkatti M, Nagarkatti PS. The role of IL-2 in the activation and expansion of
732 regulatory T-cells and the development of experimental autoimmune encephalomyelitis.
733 *Immunobiology*. 2013;218(4):674–682.
734 39. Duncker PC, et al. GM-CSF Promotes Chronic Disability in Experimental Autoimmune
735 Encephalomyelitis by Altering the Composition of Central Nervous System–Infiltrating Cells, but
736 Is Dispensable for Disease Induction. *J Immunol*. 2018;200(3):966–973.
737 40. Yosef N, et al. Dynamic regulatory network controlling TH17 cell differentiation. *Nature*.
738 2013;496(7446):461–468.
739 41. Ikegami I, et al. Bob1 enhances RORγt-mediated IL-17A expression in Th17 cells through
740 interaction with RORγt. *Biochem Biophys Res Commun*. 2019;514(4):1167–1171.
741 42. Baker D, et al. Autoimmune encephalomyelitis in NOD mice is not initially a progressive
742 multiple sclerosis model. *Ann Clin Transl Neurol*. 2019;6(8):acn3.792.
743 43. Macnair W, et al. snRNA-seq stratifies multiple sclerosis patients into distinct white matter
744 glial responses. *Neuron*. 2025;113(3):396-410.e9.

745 44. Sumida TS, et al. An autoimmune transcriptional circuit drives FOXP3+ regulatory T cell
746 dysfunction. *Sci Transl Med*. 2024;16(762):eadp1720.
747 45. Rumble JM, et al. Neutrophil-related factors as biomarkers in EAE and MS. *J Exp Med*.
748 2015;212(1):23–35.
749 46. Kroenke MA, et al. IL-12– and IL-23–modulated T cells induce distinct types of EAE based
750 on histology, CNS chemokine profile, and response to cytokine inhibition. *J Exp Med*.
751 2008;205(7):1535–1541.
752 47. Grifka-Walk HM, Lalor SJ, Segal BM. Highly polarized Th17 cells induce EAE via a T-bet
753 independent mechanism. *Eur J Immunol*. 2013;43(11):2824–2831.
754 48. Schnell A, et al. Stem-like intestinal Th17 cells give rise to pathogenic effector T cells during
755 autoimmunity. *Cell*. 2021;184(26):6281-6298.e23.
756 49. La Manno G, et al. RNA velocity of single cells. *Nature*. 2018;560(7719):494–498.
757 50. Alpsoy A, et al. IκBζ is a dual-use coactivator of NF-κB and POU transcription factors. *Mol*
758 *Cell*. [published online ahead of print: February 24, 2024].
759 https://doi.org/10.1016/j.molcel.2024.01.007.
760 51. Wu XS, et al. OCA-T1 and OCA-T2 are coactivators of POU2F3 in the tuft cell lineage.
761 *Nature*. 2022;607(7917):169–175.
762 52. Schubart DB, et al. B-cell-specif ic coactivator OBF-1/OCA-B/Bob1 required for immune
763 response and germinal centre formation. *Nature*. 1996;383(6600):538–542.
764 53. Qin XF, et al. OCA-B integrates B cell antigen receptor-, CD40L- and IL 4-mediated signals
765 for the germinal center pathway of B cell development. *EMBO J*. 1998;17(17):5066–75.
766 54. Heng TSP, et al. The Immunological Genome Project: networks of gene expression in
767 immune cells. *Nat Immunol*. 2008;9(10):1091–1094.
768 55. Zwilling S, et al. Inducible Expression and Phosphorylation of Coactivator BOB.1/OBF.1 in T
769 Cells. *Science (80-)*. 1997;277(5323):221–225.
770 56. Hughes EP, Syage AR, Tantin D. Durable CD4+ T cell immunity: cherchez la stem. *Trends*
771 *Immunol*. 2024;45(3):158–166.
772 57. Schnell A. Stem-like T cells in cancer and autoimmunity. *Immunol Rev*. 2024;325(1):9–22.
773 58. Gearty S V., et al. An autoimmune stem-like CD8 T cell population drives type 1 diabetes.
774 *Nature*. 2022;602(7895):156–161.
775 59. Li Y, et al. Stem-like T cells are associated with the pathogenesis of ulcerative colitis in
776 humans. *Nat Immunol*. 2024;25(7):1231–1244.
777 60. Sato Y, et al. Stem-like CD4+ T cells in perivascular tertiary lymphoid structures sustain

778 autoimmune vasculitis. *Sci Transl Med*. 2023;15(712):eadh0380.
779 61. Paroni M, et al. Recognition of viral and self-antigens by T H 1 and T H 1/T H 17 central
780 memory cells in patients with multiple sclerosis reveals distinct roles in immune surveillance and
781 relapses. *J Allergy Clin Immunol*. 2017;140(3):797–808.
782 62. Johns TG, et al. Myelin oligodendrocyte glycoprotein induces a demyelinating
783 encephalomyelitis resembling multiple sclerosis. *J Immunol*. 1995;154(10):5536–41.
784 63. Gao Y, et al. Transcription factor EGR2 controls homing and pathogenicity of TH17 cells in
785 the central nervous system. *Nat Immunol*. 2023;24(8):1331–1344.
786 64. McRae BL, et al. Induction of active and adoptive relapsing experimental autoimmune
787 encephalomyelitis (EAE) using an encephalitogenic epitope of proteolipid protein. *J*
788 *Neuroimmunol*. 1992;38(3):229–240.
789 65. Bernard CCA, et al. Myelin oligodendrocyte glycoprotein: a novel candidate autoantigen in
790 multiple sclerosis. *J Mol Med*. 1997;75(2):77–88.
791 66. Anderson AC, et al. A Transgenic Model of Central Nervous System Autoimmunity Mediated
792 by CD4+ and CD8+ T and B Cells. *J Immunol*. 2012;188(5):2084–2092.
793 67. Dang PT, et al. Modelling MS: Chronic-Relapsing EAE in the NOD/Lt Mouse Strain. *Curr*
794 *Top Behav Neurosci*. 2015;26:143–77.
795 68. Nish SA, et al. CD4+ T cell effector commitment coupled to self-renewal by asymmetric cell
796 divisions. *J Exp Med*. 2017;214(1):39–47.
797 69. Mammadli M, et al. TCF-1 Is Required for CD4 T Cell Persistence Functions during
798 AlloImmunity. *Int J Mol Sci*. 2023;24(5):4326.
799 70. Kadowaki A, et al. Gut microbiota-dependent CCR9+CD4+ T cells are altered in secondary
800 progressive multiple sclerosis. *Brain*. 2019;142(4):916–931.
801 71. Thakore PI, et al. BACH2 regulates diversification of regulatory and proinflammatory
802 chromatin states in TH17 cells. *Nat Immunol*. [published online ahead of print: July 15, 2024].
803 https://doi.org/10.1038/s41590-024-01901-1.
804 72. Song S, et al. OBF1 and Oct factors control the germinal center transcriptional program.
805 *Blood*. 2021;137(21):2920–2934.
806 73. Sha Y, Markovic-Plese S. Activated IL-1RI Signaling Pathway Induces Th17 Cell
807 Differentiation via Interferon Regulatory Factor 4 Signaling in Patients with Relapsing-Remitting
808 Multiple Sclerosis. *Front Immunol*. 2016;7. https://doi.org/10.3389/fimmu.2016.00543.
809 74. Lane TE, et al. A central role for CD4(+) T cells and RANTES in virus-induced central
810 nervous system inflammation and demyelination. *J Virol*. 2000;74(3):1415–24.

811 75. Blanc CA, et al. Sphingosine-1-Phosphate Receptor Antagonism Enhances Proliferation and
812 Migration of Engrafted Neural Progenitor Cells in a Model of Viral-Induced Demyelination. *Am J*
813 *Pathol*. 2015;185(10):2819–2832.
814 76. Plaisted WC, et al. Remyelination Is Correlated with Regulatory T Cell Induction Following
815 Human Embryoid Body-Derived Neural Precursor Cell Transplantation in a Viral Model of
816 Multiple Sclerosis. *PLoS One*. 2016;11(6):e0157620.
817 77. Keeler GD, et al. Gene Therapy-Induced Antigen-Specific Tregs Inhibit Neuro-inflammation
818 and Reverse Disease in a Mouse Model of Multiple Sclerosis. *Mol Ther*. 2018;26(1):173–183.
819 78. Tu E, et al. T Cell Receptor-Regulated TGF-β Type I Receptor Expression Determines T
820 Cell Quiescence and Activation. *Immunity*. 2018;48(4):745-759.e6.
821 79. Dickey LL, et al. MicroRNA-155 enhances T cell trafficking and antiviral effector function in a
822 model of coronavirus-induced neurologic disease. *J Neuroinflammation*. 2016;13(1):240.
823

824 Figure legends

825 **Figure 1. OCA-B loss protects animals from chronic EAE.** (**A**) CD4$^+$ T cell nuclei from single-
826 nucleus RNAseq data of primary-progressive (PPMS), relapsing-remitting MS (RRMS), and
827 secondary-progressive MS (SPMS) patient lesions and controls (43) were identified and tested in
828 silico for *POU2AF1* expression, which is displayed as counts per million. Significance was
829 ascribed by Welch's T-test. (**B**) The CD4$^+$ T cell nuclei were reclustered and displayed as UMAP
830 feature plots showing *POU2AF1* (left) and *IL1R1* (right) expression in CTR and SPMS brain
831 tissue. Red arrow highlights a likely pathogenic CD4$^+$ population expressing high levels of *IL1R1*.
832 (**C**) *Ocab*$^{fl/fl}$ (n=16) and *Ocab*$^{fl/fl}$;CD4-Cre (n=22) mice were injected with MOG$_{35-55}$ peptide in CFA
833 and *pertussis* toxin to induce EAE. Clinical scores were evaluated after EAE induction to
834 determine disease progression. (**D**) Animal weights were recorded to evaluate weight loss as a
835 measurement of disease progression. (**E**) Representative DAPI/MBP immunostaining of thoracic
836 spinal cord sections taken from mice 15 days after EAE induction. Areas of demyelination are
837 marked by decreased MBP staining (green) and often coincide with increased cellular infiltration
838 (blue). (**F**) Quantification of demyelination in *Ocab*$^{fl/fl}$ (n=5) and *Ocab*$^{fl/fl}$;CD4-Cre mice (n=6). (**G**)
839 Brain and spinal cords were isolated on day 15 of EAE and analyzed by spectral cytometry.
840 Representative flow cytometry plots of CD45$^+$TCRβ^+ CNS infiltrating T cells showing frequency of
841 CD4$^+$ and CD8$^+$ T cells. (**H**) Quantification of the number of CNS infiltrating CD4$^+$ T cells. *Ocab*$^{fl/fl}$
842 (n=9) and *Ocab*$^{fl/fl}$;CD4-Cre (n=13). (**I**) Representative plots showing frequency of MOG$_{38-49}$
843 tetramer-positive CD4$^+$ T cells. (**J**) Quantification of the frequency and count of MOG$_{38-49}$ tetramer-
844 positive CD4$^+$ T cells. *Ocab*$^{fl/fl}$ (n=9) and *Ocab*$^{fl/fl}$;CD4-Cre (n=13). For clinical scores and
845 normalized weights, values represent mean ±SEM. All other values represent mean ±SD.

846

847 **Figure 2. OCA-B promotes Th1 and Th17 adoptive transfer EAE through recall response.**
848 (**A,B**) *Ocab*$^{fl/fl}$ and *Ocab*$^{fl/fl}$;CD4-Cre mice were primed with MOG$_{35-55}$ peptide in CFA for 10-14
849 days. Cells from the spleens and lymph nodes of primed mice were isolated and cultured for 4
850 days in Th1 or Th17 polarizing conditions. 3.0x10^6 Th1- or Th17-polarized cells were injected i.p.
851 into C57BL/6 wildtype recipient mice (Th1: *Ocab*$^{fl/fl}$ n=5, *Ocab*$^{fl/fl}$;CD4-Cre n=5) (Th17: *Ocab*$^{fl/fl}$
852 n=3, *Ocab*$^{fl/fl}$;CD4-Cre n=4). Clinical scores were assessed for 14-15 days. (**C**) At Th17 adoptive
853 transfer EAE endpoint, brains and spinal cords were analyzed by flow cytometry. Quantification
854 of brain- and spinal cord-infiltrating CD4$^+$ T cells following Th17 adoptive transfer. (**D**)
855 Representative flow cytometry plots showing the frequency of IFNγ and IL-17 expressing CD4$^+$ T

856 cells within the spines of Th17 recipient mice. (**E**) Quantification of IL-17 frequency in spinal cord
857 infiltrating CD4$^+$ T cells. (**F**) Quantification of the total count of IL-17$^+$ CD4$^+$ T cells within the spinal
858 cord of recipient mice. For clinical scores, values represent mean ±SEM. All other values
859 represent mean ±SD.
860
861
862 **Figure 3. OCA-B is dispensable for T cell response to CNS infection with a neurotropic**
863 **virus.** (**A**) *Ocab*$^{fl/fl}$ (n=19) and *Ocab*$^{fl/fl}$;CD4-Cre (n=17) mice were injected intracranially with 1500
864 PFU JHMV. Clinical scores were recorded for 21 days post infection (dpi). (**B**) Representative
865 DAPI/MBP immunofluorescence staining of spinal cord sections at 12 dpi. Demyelinated areas
866 are marked by decreased MBP staining (green) and often coincide with increased cellular
867 infiltration (blue). (**C**) Quantification of % demyelination in spinal cord sections. (n=7 per group).
868 Half brains were taken at 7, 12, and 21 dpi for flow cytometric and viral titer analysis. (**D**)
869 Quantification of CD4$^+$ T cell counts within half brain at 7, 12, 21 dpi. *Ocab*$^{fl/fl}$ (n=7-9 per time
870 point) and *Ocab*$^{fl/fl}$;CD4-Cre (n=6-7 per time point). (**E**) Representative plots showing the
871 frequency of IFNγ expressing CD4$^+$ T cells 7, 12, and 21 dpi. (**F**) Quantification of frequency of
872 IFNγ expressing CD4$^+$ T cells. *Ocab*$^{fl/fl}$ (n=7-9 per time point) and *Ocab*$^{fl/fl}$;CD4-Cre (n=6-7 per
873 time point). (**G**) Viral titers of half-brains at dpi 7, 12, and 21 (n.d., not detected). *Ocab*$^{fl/fl}$ (n=7-9
874 per time point) and *Ocab*$^{fl/fl}$;CD4-Cre (n=6-7 per time point). These data represent the combined
875 results of two independent experiments. For clinical scores, values represent mean ±SEM. All
876 other values represent mean ±SD.
877
878 **Figure 4. OCA-B expression marks encephalitogenic stem-like CD4$^+$ T cells.** (**A**) OCA-B-
879 mCherry mice were injected with MOG$_{35-55}$ peptide in CFA and *pertussis* toxin to induce EAE.
880 Cervical lymph nodes (CLNs), brains, and spines were isolated at peak disease (day 15) and
881 analyzed by flow cytometry for mCherry, CD44 and CD62L expression. (**B**) CD44$^+$ and CD62L$^+$
882 expressing CD4$^+$ T cells were quantified based on mCherry expression. Mean values are shown
883 from n=5 biological replicates. (**C**) OCA-B-mCherry mice were injected with MOG$_{35-55}$ peptide in
884 CFA, and after 14 days CD4$^+$ T cells within CLNs and spleens were profiled by flow cytometry for
885 mCherry, CD44, and CD62L expression. (**D**) Quantification of CD44 and CD62L expression of
886 OCA-B negative and positive CD4$^+$ T cells from MOG-primed OCA-B-mCherry mice. n=4-6
887 biological replicates from two combined replicate experiments are shown. (**E**) Heatmap showing

888 relative expression of the top 40 differentially expressed genes from OCA-B positive and negative
889 $CD4^+$ T cells from bulk RNA sequencing of OCA-B positive and negative $CD4^+$ T cells from MOG_{35-}
890 $_{55}$ primed OCA-B-mCherry reporter mice. (**F**) Volcano plot of differentially expressed genes
891 between OCA-B positive and negative T cells (*p*-value < 0.05 and Log2 fold change > 1 are
892 colored). (**G**) Gene Ontology (GO) terms associated with OCA-B positive and negative groups.
893 (**H**) EAE clinical scores of C57BL/6 wild-type mice following passive transfer of OCA-B-positive
894 or -negative Th1 polarized $CD4^+$ T cells. Clinical score values represent mean ±SEM. All other
895 values represent mean ±SD.
896
897 **Figure 5. OCA-B promotes relapsing-remitting EAE through stem-like $CD4^+$ T cells.** (**A**)
898 NOD.*Ocab*$^{fl/fl}$ (n=19) and NOD.*Ocab*$^{fl/fl}$;CD4-Cre (n=15) mice were injected with MOG_{35-55} peptide
899 in CFA and *pertussis* toxin to induce EAE. Clinical scores of animals representing relapsing-
900 remitting disease progression are shown as a function of time. (**B**) Animal weights were recorded
901 to determine weight loss throughout initial disease and relapse. (**C**) Singe cell RNA sequencing
902 was performed on pooled $CD3\varepsilon^+$ cells isolated from the brain and spine of NOD.*Ocab*$^{fl/fl}$ (n=3) and
903 NOD.*Ocab*$^{fl/fl}$;CD4-Cre (n=4) 24 days after EAE induction (remission timepoint). Cell populations
904 were plotted in a UMAP using the Seurat R package and percentages are shown for each cluster.
905 Clusters were identified through differential gene expression analysis. (**D**) Feature plots
906 comparing the expression of *Foxp3* and *Mki67* amongst clusters. (**E**) Violin plots showing the
907 expression of *Btg1*, *Samhd1*, *Slamf6*, *Tcf7, Sell* and *Tox* within the Treg, proliferating, and Th1-
908 like clusters. (**F**) CNS cells isolated at remission timepoint (day 24) were analyzed by spectral
909 cytometry. Representative flow cytometry plots and quantification showing the frequency of $CD4^+$
910 T cells between control and experimental groups. (**G**) Representative flow cytometry plots and
911 quantification showing the frequency of CXCR6 expressing $CD4^+$ T cells. (**H**) Representative flow
912 cytometry plots showing the frequency of $CD4^+$ T cells expressing IFNγ and GM-CSF. (**I**)
913 Quantification of $CD4^+$ T cells expressing IFNγ and GM-CSF. For clinical scores, data represent
914 mean ±SEM. All other data represents mean ±SD.
915
916 **Figure 6. OCA-B promotes disease relapse through control of pathogenic stem-like Th17**
917 **differentiation.** (**A**) Singe cell RNA and TCR sequencing were performed on pooled $CD3\varepsilon^+$ cells
918 isolated from the brain and spine of NOD.*Ocab*$^{fl/fl}$ (n=5) and NOD.*Ocab*$^{fl/fl}$;CD4-Cre (n=6) 33 days
919 after EAE induction (relapse timepoint). Cell populations were plotted in a UMAP using the Seurat

920 R package and percentages are shown for each cluster. Clusters were identified through
921 differential gene expression analysis. (**B**) UMAP TCR clonotype expansion between *Ocab*$^{fl/fl}$ and
922 *Ocab*$^{fl/fl}$;CD4-Cre amongst clusters. (**C**) Violin plots showing expression of *Ccr9*, *Bach2*, *Ccr7*,
923 *Tcf7*, *Cd44*, *Cxcr6*, *Il1r1* and *Lgals3* in the Ccr9 Stem-like CD4, Stem-like CD4-2, and Th17-like
924 clusters. (**D**) Feature plots comparing the expression of *Ccr9*, *Tcf7*, and *Bach2* amongst clusters**.**
925 (**E**) UMAPs showing RNA velocity of spliced and unspliced transcripts by experimental condition.
926 (**F**) Violin plots showing expression of *Pdcd1*, *Tigit*, and *Il1r1* in the Th17-like cluster between
927 control and experimental groups.

928 Supplemental figure legends

929 **Supplemental Figure 1. Reclustered CD4$^+$ nuclei gene expression and analysis of**
930 **peripheral blood CD4$^+$ T effector cell bulk RNAseq .** (**A**) Additional feature plots of reclustered
931 CD4$^+$ T cell nuclei from single-nucleus RNAseq data of secondary-progressive MS (SPMS)
932 patient lesions and controls (43) showing cluster gene expression of *CD4*, *CD44*, *LEF1*, *ETS1*,
933 *BCL6*, and *MAF*. (**B**) Quantification of *POU2AF1* counts from bulk RNAseq data of CD4$^+$ T effector
934 cells isolated from the peripheral blood of control (HC Teff) and MS (MS Teff) patients (44). All
935 data represent mean ±SD and Welch's T-test was used to determine statistical significance for
936 data with unequal variance.

937

938 **Supplemental Figure 2. Minimal differences in cytokine expressing CD4$^+$ T cell, CD8$^+$ T cell,**
939 **B cell, macrophage or microglial cell counts at peak chronic EAE in OCA-B knockouts.** (**A**)
940 Representative spinal cord LFB/H&E staining of thoracic sections taken from mice 15 days after
941 EAE induction. Areas of demyelination are outlined in black and marked by increased loss of LFB
942 (blue) staining and visibility of H&E (pink) within the white matter. (**B**) Quantification of the %
943 demyelination from LFB/H&E histology. (**C**) Quantification of the frequency of CNS infiltrating
944 CD4$^+$ T cells between Ocab$^{fl/fl}$ and Ocab$^{fl/fl}$;CD4-Cre mice. (**D**) Quantification of frequency and
945 count of CD8α positive T cells between Ocab$^{fl/fl}$ and Ocab$^{fl/fl}$;CD4-Cre mice. (**E**) Quantification of
946 the number of B cells, macrophages and microglia. (**F**) Representative flow cytometry plots
947 comparing the expression of FR4 and CD73 within CNS infiltrating CD4$^+$ T cells from Ocab$^{fl/fl}$ and
948 Ocab$^{fl/fl}$;CD4-Cre mice. (**G**) Quantification of the frequency of CNS infiltrating FR4$^+$ CD73$^-$ and
949 FR4$^+$ CD73$^+$ CD4$^+$ T cells within Ocab$^{fl/fl}$ and Ocab$^{fl/fl}$;CD4-Cre mice. (**H**) Quantification of
950 frequency and count of IFNγ, IL-17, GM-CSF, and CD44 expressing CD4$^+$ T cells from Ocab$^{fl/fl}$
951 and Ocab$^{fl/fl}$;CD4-Cre mice. All data represent mean ±SD.

952

953 **Supplemental Figure 3. Loss of OCA-B does not strongly alter initial Th1 or Th17**
954 **polarization in vitro.** (**A**) Experimental schematic for assessing CD4$^+$ T cell differences between
955 Ocab$^{fl/fl}$ and Ocab$^{fl/fl}$CD4-Cre prior to *in vitro* Th1 or Th17 polarization. Lymph nodes (cervical,
956 brachial, axillary, and inguinal) were harvested from Ocab$^{fl/fl}$ (n=4) and Ocab$^{fl/fl}$;CD4-Cre (n=4)
957 mice following 14 days of MOG$_{35-55}$/CFA priming and analyzed by flow cytometry. (**B**) Frequency
958 of viable cells isolated from Ocab$^{fl/fl}$ and Ocab$^{fl/fl}$;CD4-Cre mice. (**C**) Total CD4$^+$ T cell numbers
959 isolated from Ocab$^{fl/fl}$ and Ocab$^{fl/fl}$;CD4-Cre mice. (**D**) Quantification of the frequency of IFNγ

960 expressing CD4$^+$ T cells isolated from Ocab$^{fl/fl}$ and Ocab$^{fl/fl}$;CD4-Cre mice. (**E**) Quantification of
961 the frequency of IL-17 expressing CD4$^+$ T cells derived from Ocab$^{fl/fl}$ and Ocab$^{fl/fl}$;CD4-Cre mice.
962 (**F**) Normalized weights of recipient mice following adoptive transfer of Ocab$^{fl/fl}$ or Ocab$^{fl/fl}$;CD4-
963 Cre Th1-polarized MOG-reactive CD4$^+$ T cells. (**G**) Normalized weights of recipient mice following
964 adoptive transfer of Ocab$^{fl/fl}$ or Ocab$^{fl/fl}$;CD4-Cre Th17 cells. (**H**) Representative flow cytometry
965 plots showing IFNγ and IL-17 expressing CD4$^+$ T cells from Ocab$^{fl/fl}$ (n=5) and Ocab$^{fl/fl}$;CD4-Cre
966 (n=5) mice after Th1 and Th17 *in vitro* polarization. (**I**) Quantification of IFNγ expressing CD4$^+$ T
967 cells after Th1 polarization. (**J**) Quantification of IL-17 expressing CD4$^+$ T cells after Th17
968 polarization. (**K**) Quantification of the frequency of IFNγ expressing CD4$^+$ T cells isolated from the
969 spinal cords of Th17 adoptive transfer EAE recipient mice. Normalized weight variance is
970 displayed as mean ±SEM. All other data represent mean ±SD.
971
972 **Supplemental Figure 4. Minimal changes in immune responses to intracranial JHMV**
973 **infection in the absence of OCA-B.** (**A**) Representative LFB/H&E histology of spinal cord
974 sections at dpi 21. (**B**) Demyelination quantification of LFB/H&E histology at dpi 21. (**C**)
975 Quantification of the number of IFNγ expressing CD4$^+$ T cells at dpi 7, 12 and 21. (**D**)
976 Quantification of the number of CD8$^+$ T cells at dpi 7, 12 and 21. (**E**) Quantification of the frequency
977 of IFNγ expressing CD8$^+$ T cells at dpi 7, 12 and 21. (**F**) Quantification of the number of IFNγ
978 expressing CD8$^+$ T cells at dpi 7, 12 and 21. All data represent mean ±SD.
979
980 **Supplemental Figure 5. Sorting OCA-B-mCherry reporter T cells and additional analysis of**
981 **the effects of transferring OCA-B^{hi} versus OCA-B^{lo} CD4$^+$ cells.** (**A**) Quantification of the
982 frequency of CD44$^+$ CD62$^-$ CD4$^+$ T cells within the cervical lymph nodes of OCA-B-mCherry
983 reporter mice at peak EAE by OCA-B-mCherry expression. (**B**) Gating strategy for sorting of OCA-
984 B$^+$ and OCA-B$^-$ CD4$^+$ T cells. (**C**) *mm39* ChIP-seq tracks showing peaks for Oct1 (blue), OCA-B
985 (red), along with vertebrate conservation (black) at *Tcf7*, *Bcl6*, and *Bach2*. (**D**) Normalized weights
986 of recipient mice following adoptive transfer of Ocab mCherry positive or negative Th1 cells.
987 Normalized weight is represented by mean ±SEM. All other data represent mean ±SD.
988
989 **Supplemental Figure 6. Individual NOD mouse EAE clinical scores.** (**A**) Clinical scores of
990 individual NOD.Ocab$^{fl/fl}$ mice following EAE induction. (**B**) Clinical scores of individual
991 NOD.Ocab$^{fl/fl}$;CD4-Cre mice following EAE induction.

992

993 **Supplemental Figure 7. Additional remission scRNA-seq cluster annotation, heat map of**
994 **gene enrichments by cluster, and additional feature plots.** (**A**) Violin plots showing cluster
995 gene expression of *CD3e*, *Cd4*, *Cd8a*, *Ncr1*(NKp46), *Cxcr6*, *Tcf7*, and *Tcrg-V6* at EAE remission
996 (**B**) Heatmap showing the top 10 genes expressed by cluster at remission EAE timepoint. (**C**)
997 UMAP feature plots showing expression of *Cxcr6*, *Il23r*, and *Bach2* amongst clusters at remission.
998

999 **Supplemental Figure 8. scRNA-seq cluster annotation genes, heat map of NOD.EAE gene**
1000 **enrichments by cluster, and TCR clonotype overlap between conditions at the relapse**
1001 **timepoint.** (**A**) Violin plots showing cluster gene expression of *CD3e*, *Cd4*, *Cd8a*, *Ncr1*(NKp46),
1002 *Cxcr6*, *Tcf7*, and *Tcrg-V6* at EAE relapse. (**B**) Heatmap showing the top 10 genes expressed by
1003 cluster at relapse EAE timepoint. (**C**) Alluvial plot showing top 10 TCR clonotype gene overlap
1004 between Ocab$^{fl/fl}$ and Ocab$^{fl/fl}$;CD4-Cre groups. (**C**) UMAP feature showing the expression of *CD4*,
1005 *CD8a, Tox*, *Sell*, *Ccr7*, and *Ccr4* amongst clusters at relapse timepoint.
1006

1007 **Supplemental Figure 9. Example relapse feature plots and pseudotime analysis of relapse**
1008 **single cell RNA seq.** (**A**) UMAP feature showing the expression of *CD4*, *CD8a, Tox*, *Sell*, *Ccr7*,
1009 and *Ccr4* amongst clusters at relapse timepoint. (**B**) Pseudotime analysis of relapse single cell
1010 from root starting node at or near the *Ccr9*-expressing stem-like cluster.

Hughes et al. Figure 1

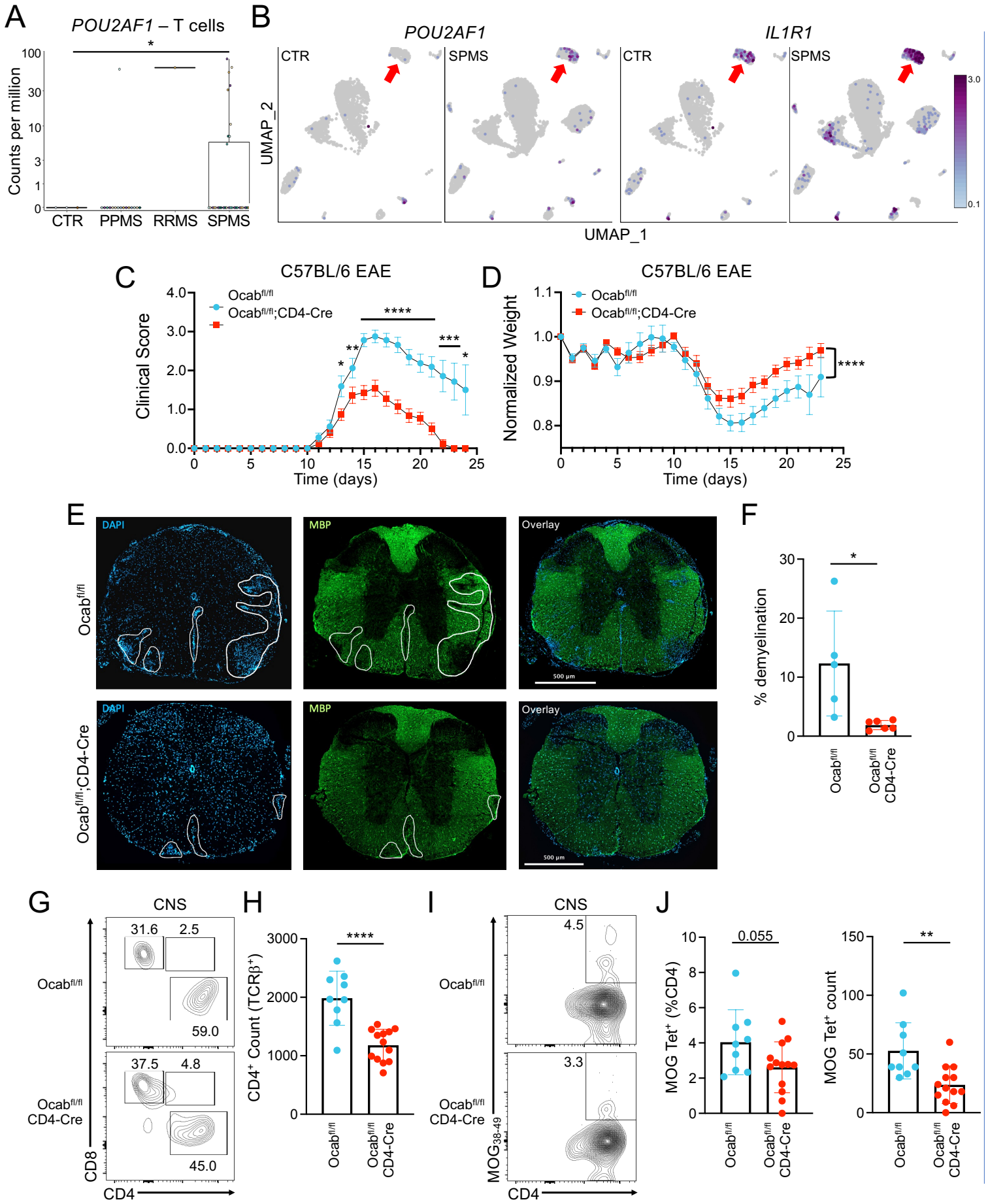

Hughes et al. Figure 2

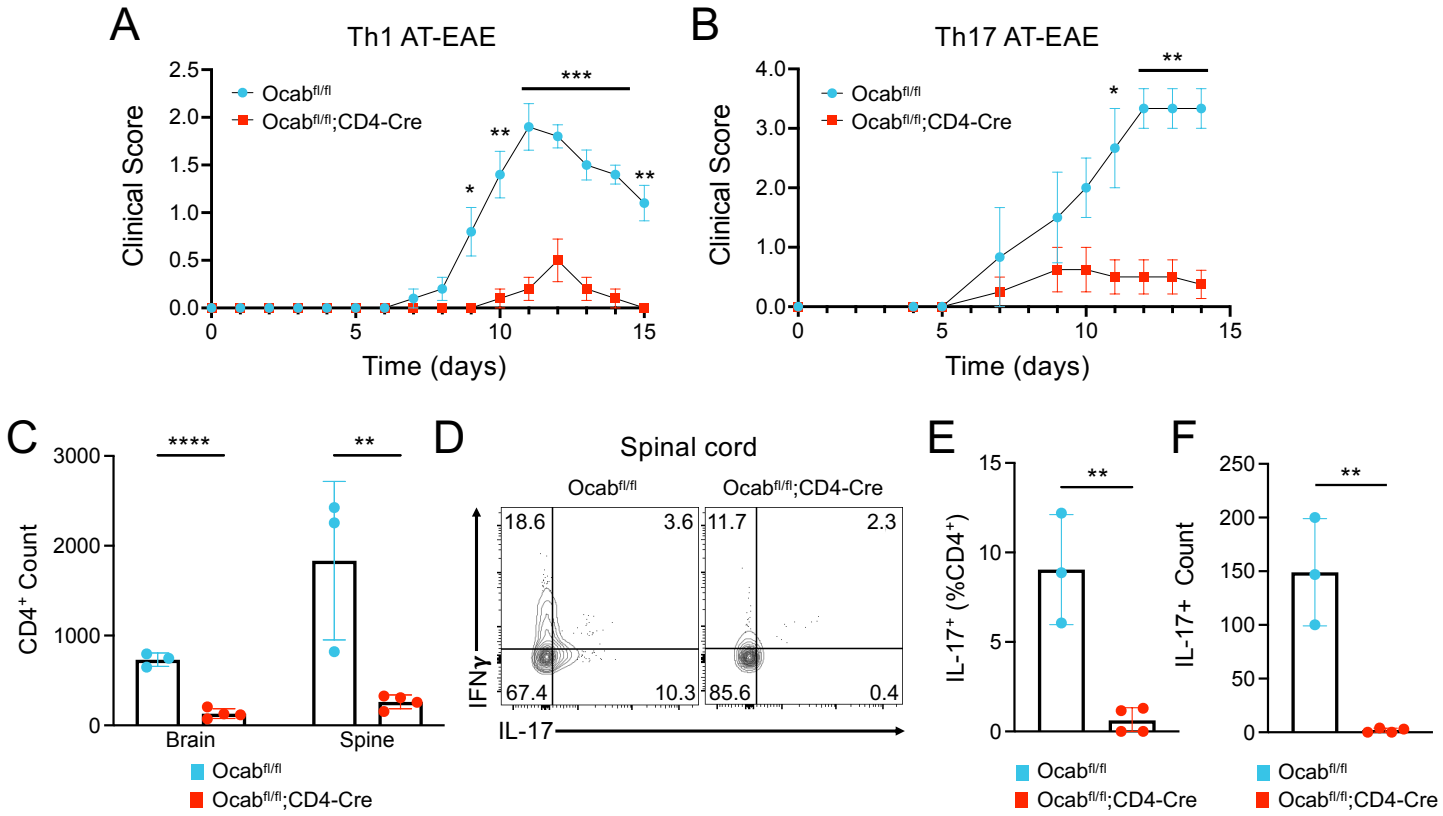

Hughes et al. Figure 3

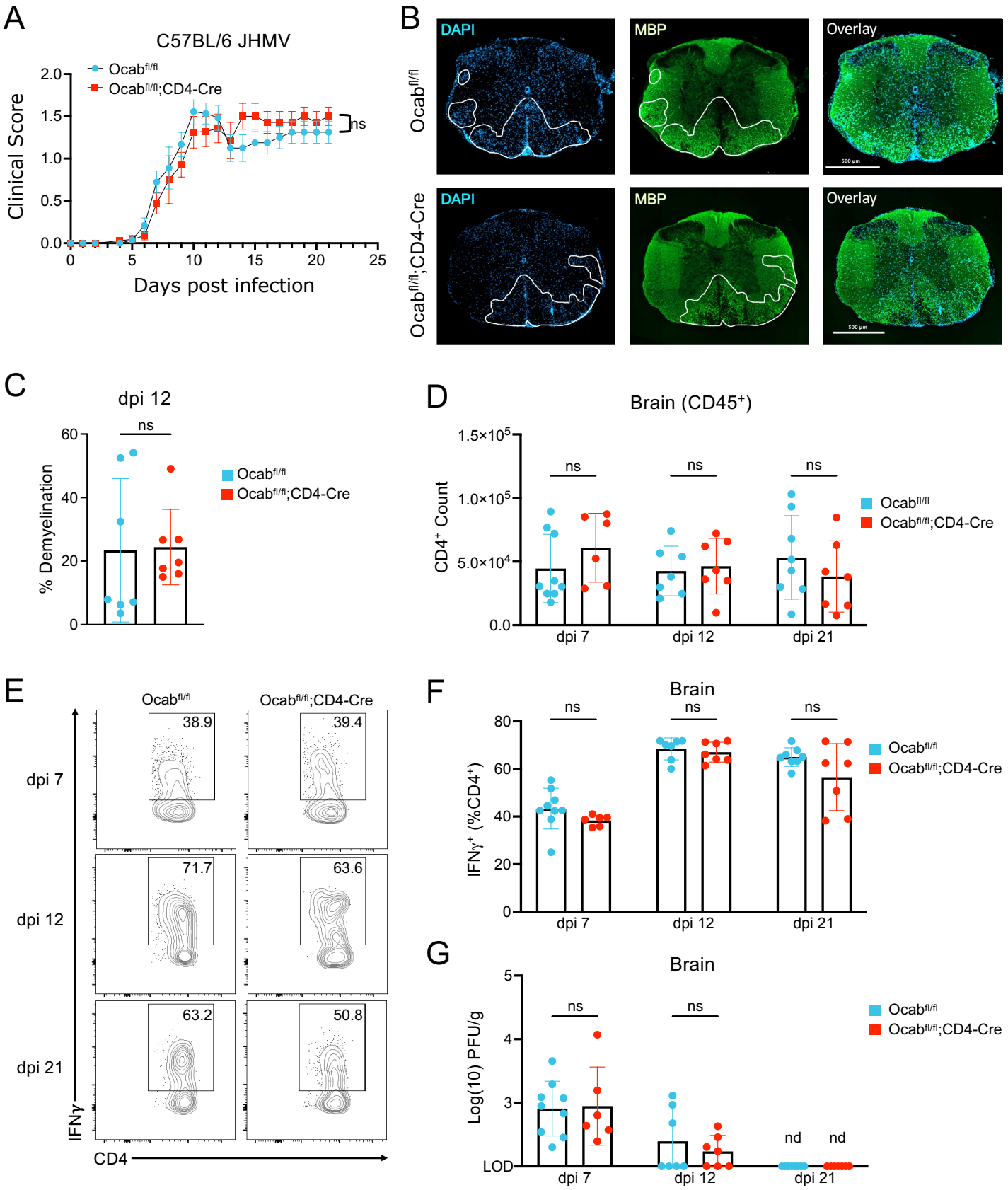

Hughes et al. Figure 4

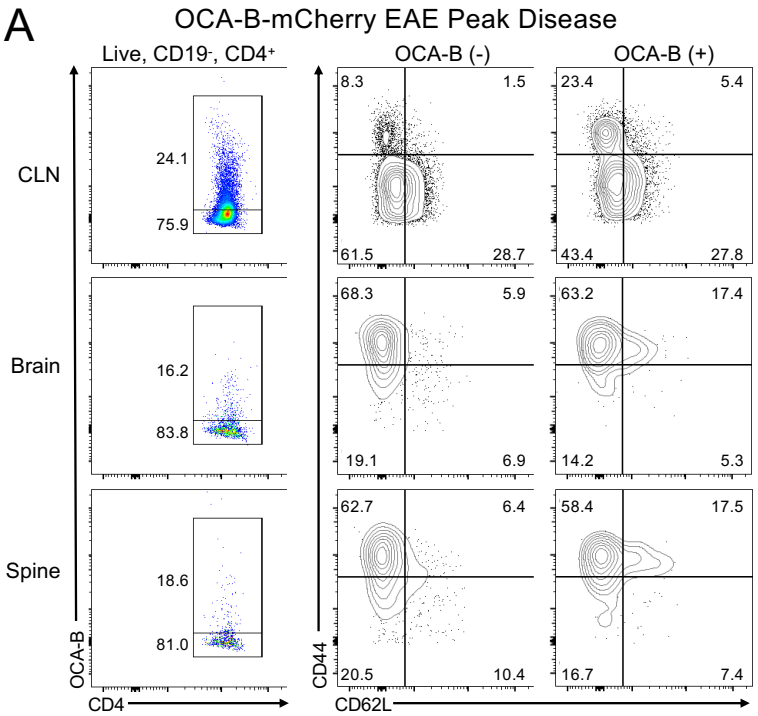

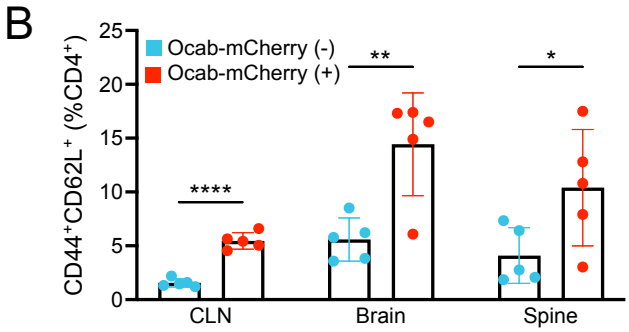

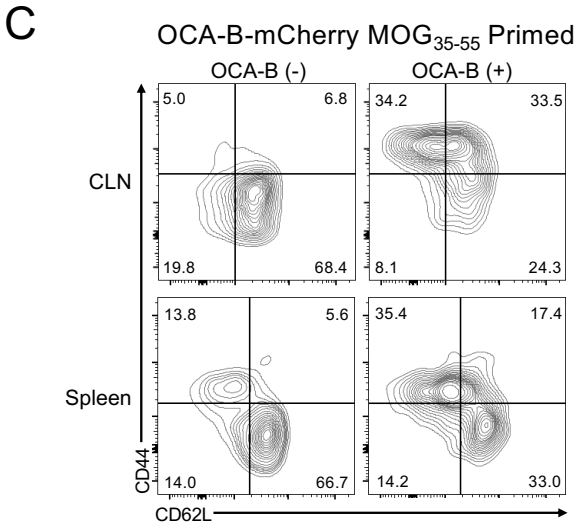

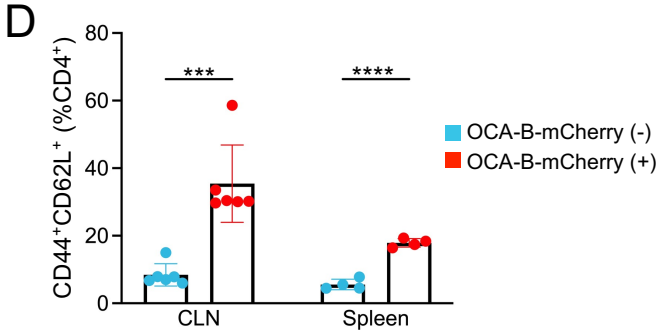

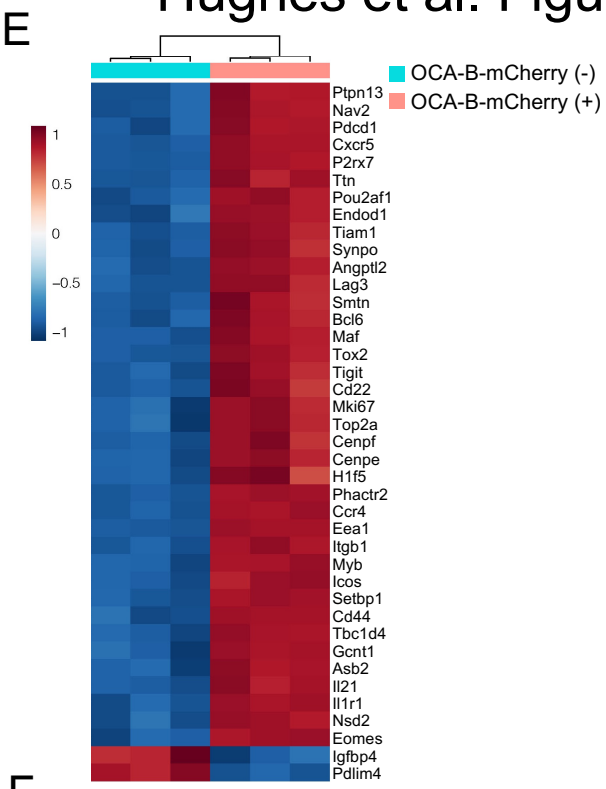

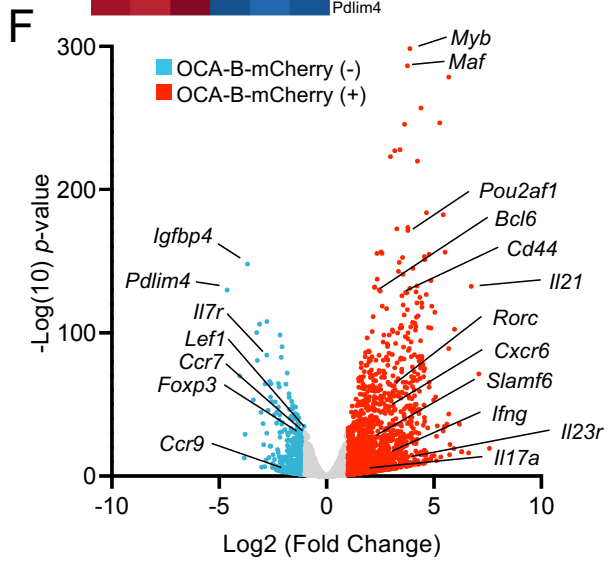

G

OCA-B+ Enriched Pathways

KEGG Pathway	*p*-value
Systemic Lupus Erythematosus	1.02E-04
Cytokine Cytokine Receptor Interaction	5.04E-04
Autoimmune Thyroid Disease	1.16E-03
Type I Diabetes Mellitus	2.06E-03

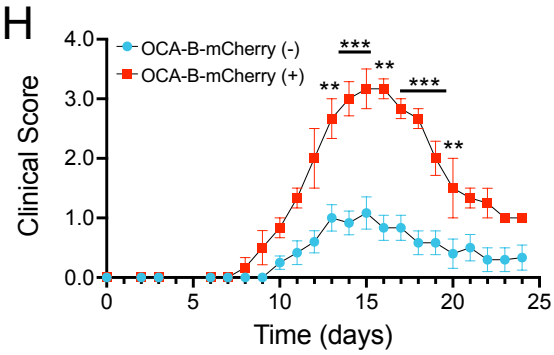

Hughes et al. Figure 5

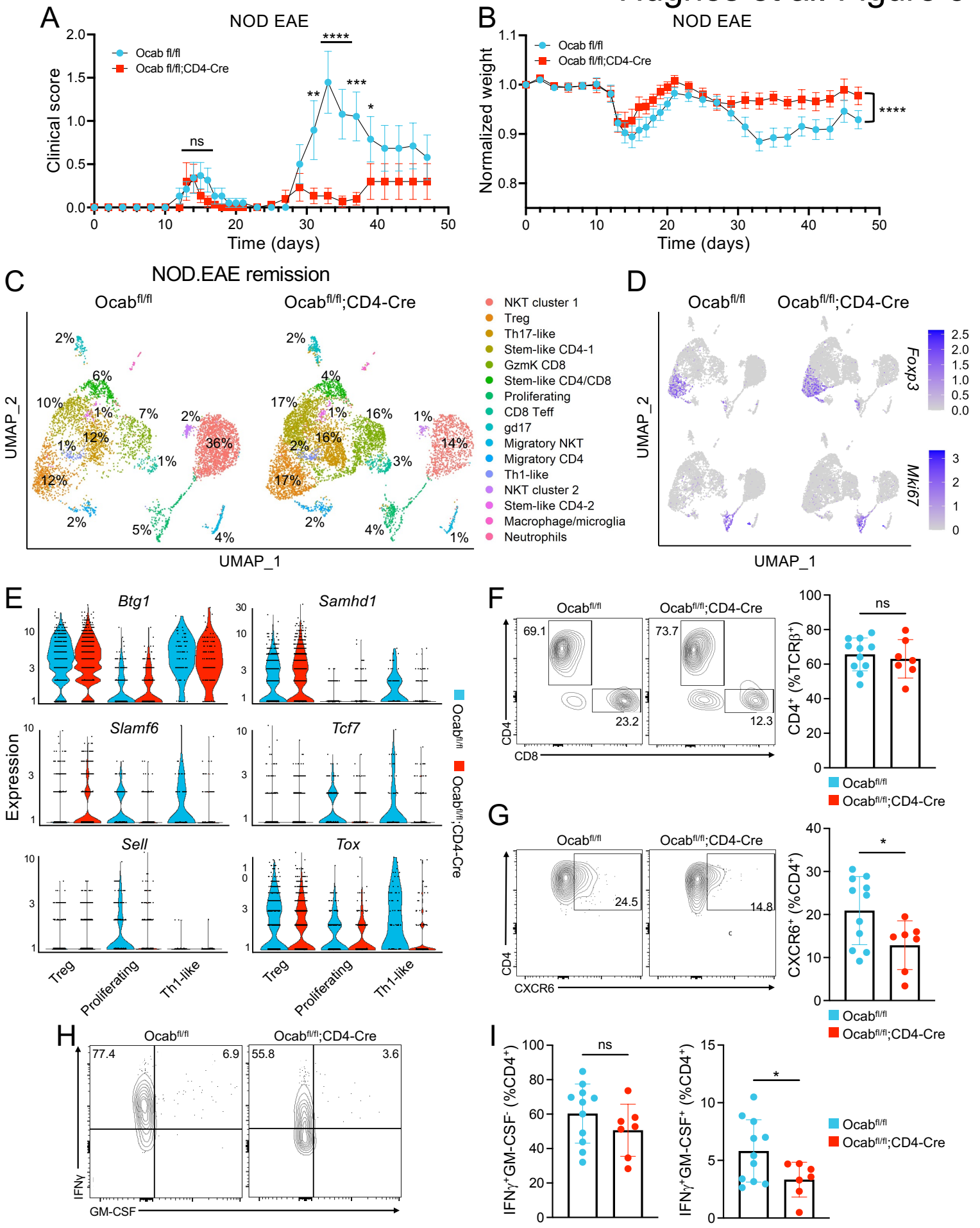
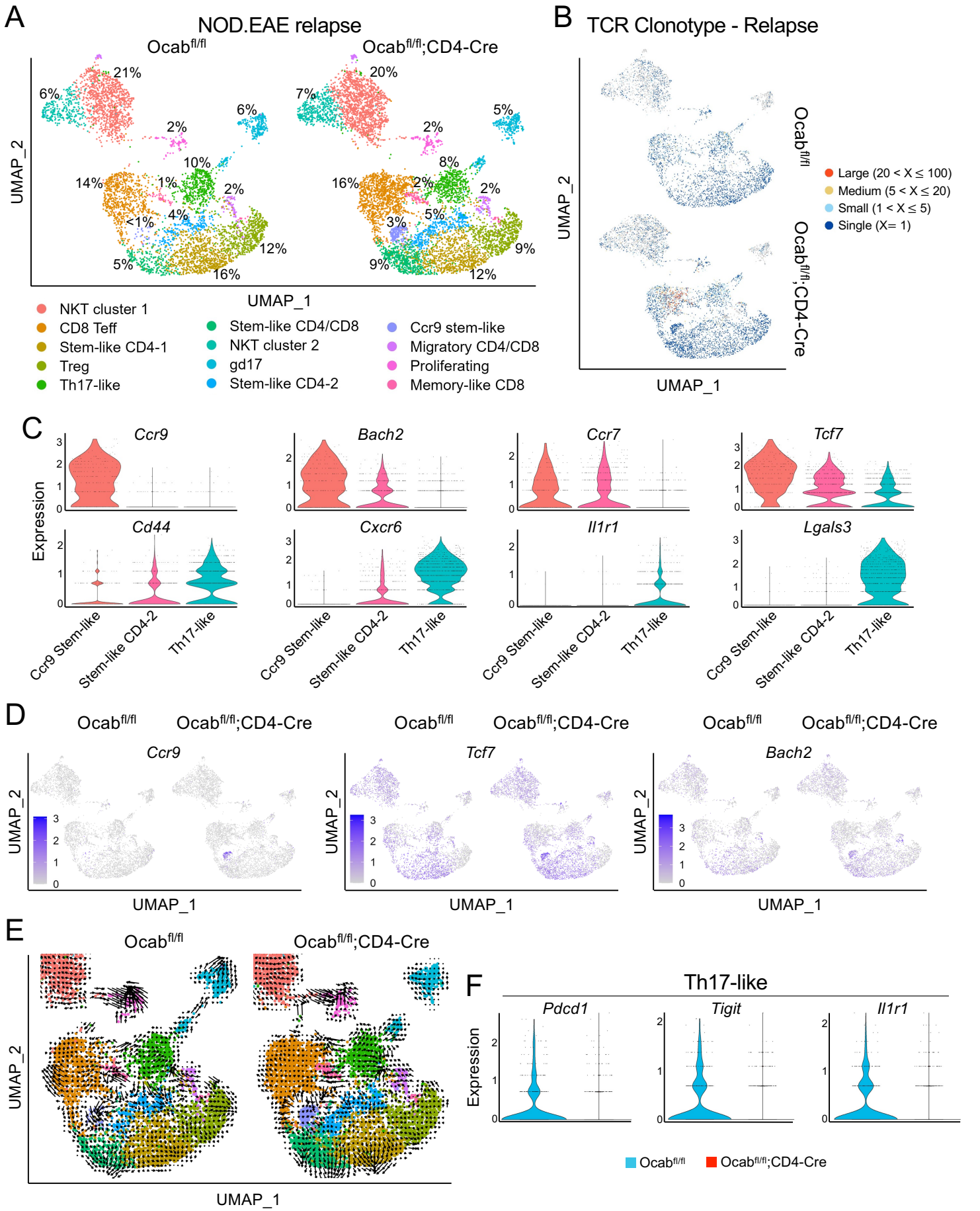
Hughes et al. Figure 6